THE JOURNAL OF BIOLOGICAL CHEMISTRY VOL. 288, NO. 34, pp. 24609–24624, August 23, 2013

Structural and Functional Analysis of Transmembrane Segment IV of the Salt Tolerance Protein Sod2*[S]

Received for publication, May 4, 2013, and in revised form, June 25, 2013 Published, JBC Papers in Press, July 8, 2013, DOI 10.1074/jbc.M113.483065

Asad Ullah, Grant Kemp[1], Brian Lee[2], Claudia Alves, Howard Young[3], Brian D. Sykes, and Larry Fliegel[4]

From the Department of Biochemistry, University of Alberta, Edmonton, Alberta T6G 2H7, Canada

Background: Sod2 is the salt tolerance protein of *Schizosaccharomyces pombe*.
Results: Alanine scanning mutagenesis and structural analysis demonstrated that amino acids 144–147 are in an extended region of transmembrane segment IV and are critical for function.
Conclusion: Mutations in transmembrane segment IV affect Sod2 cation transport.
Significance: TM IV of Sod2 has conserved structures with other Na^+/H^+ exchangers important in salt tolerance.

Sod2 is the plasma membrane Na^+/H^+ exchanger of the fission yeast *Schizosaccharomyces pombe*. It provides salt tolerance by removing excess intracellular sodium (or lithium) in exchange for protons. We examined the role of amino acid residues of transmembrane segment IV (TM IV) (^{126}FPQINFLGSLLIAGCITSTDPVLSALI^{152}) in activity by using alanine scanning mutagenesis and examining salt tolerance in *sod2*-deficient *S. pombe*. Two amino acids were critical for function. Mutations T144A and V147A resulted in defective proteins that did not confer salt tolerance when reintroduced into *S. pombe*. Sod2 protein with other alanine mutations in TM IV had little or no effect. T144D and T144K mutant proteins were inactive; however, a T144S protein was functional and provided lithium, but not sodium, tolerance and transport. Analysis of sensitivity to trypsin indicated that the mutations caused a conformational change in the Sod2 protein. We expressed and purified TM IV (amino acids 125–154). NMR analysis yielded a model with two helical regions (amino acids 128–142 and 147–154) separated by an unwound region (amino acids 143–146). Molecular modeling of the entire Sod2 protein suggested that TM IV has a structure similar to that deduced by NMR analysis and an overall structure similar to that of *Escherichia coli* NhaA. TM IV of Sod2 has similarities to TM V of the *Zygosaccharomyces rouxii* Na^+/H^+ exchanger and TM VI of isoform 1 of mammalian Na^+/H^+ exchanger. TM IV of Sod2 is critical to transport and may be involved in cation binding or conformational changes of the protein.

Under normal physiological conditions, plant, yeast, and mammalian cells have relatively low Na^+ concentrations in their cytosol. Because the external Na^+ is much higher than internal Na^+, this leads to an accumulation of intracellular Na^+. Organisms respond to this salt stress in several ways. Plants and yeast deal with these excess "toxic" levels of intracellular Na^+ primarily by either extruding it or sequestering it into vacuoles, thereby reducing the cytosolic concentration. This process is mediated by transporters and other regulatory proteins. In the fission yeast *Schizosaccharomyces pombe*, the Na^+/H^+ antiporter (Sod2) is responsible for most of the salt removal from the cytosol (1). This protein functions by using the external proton gradient to pump out internal Na^+ ions. Disruption of this gene results in a reduced extrusion of cytoplasmic Na^+ and a decreased tolerance of external Na^+ (1). Sod2 removes both Na^+ and Li^+ from the cytosol using the proton gradient created by the plasma membrane ATPase (1, 2). We have previously (3, 4) used *S. pombe* with a knock-out of the *sod2* gene to study the effects of mutation of amino acids in this protein. Because of the limited number of other salt tolerance mechanisms in this species, removal of this gene results in a severe salt tolerance phenotype (1, 3, 4). This makes *S. pombe* a very useful organism for the study of salt tolerance proteins.

Sod2 belongs to the class of Na^+/H^+ exchanger membrane proteins that exchange Na^+ for H^+ ions across lipid bilayers. The eukaryotic and prokaryotic genes that encode the members of this monovalent cation/proton antiporter superfamily have been reviewed (5). Briefly, the superfamily includes three families, the cation/proton antiporter 1 family, cation/proton antiporter 2 family, and the sodium-transporting carboxylic acid decarboxylase family, each of which has unique bacterial ancestors. The cation/proton antiporter 1 family includes many well studied Na^+/H^+ exchangers including from fungi, plants, and mammals and includes the human NHE1–NHE10 isoforms. The cation/proton antiporter 2 family includes *S. pombe sod2* and shares its origins with prokaryotic NhaA, the *Escherichia coli* antiporter, for which a crystal structure has been deduced (6). This family also includes two relatively recently characterized forms of human Na^+/H^+ exchangers, HsNHA1 and HsNHA2, that may be involved in hypertension (5, 7, 8). The sodium-transporting carboxylic acid decarboxylase family

* This work was supported in part by a grant from the Natural Sciences and Engineering Research Council (to L. F.) and grants from the Canadian Institutes of Health Research (CIHR) (to H. Y. and B. D. S.).
[S] This article contains supplemental Table 1 and Figs. 1–10.
The atomic coordinates and structure factors (code 2M7X) have been deposited in the Protein Data Bank (http://wwpdb.org/).
[1] Supported by graduate scholarships from CIHR and Alberta Innovates Health Solutions (AIHS).
[2] Supported by graduate scholarships from AIHS and the Heart and Stroke Foundation of Canada.
[3] Supported by awards from AIHS.
[4] Supported by awards from AIHS. To whom correspondence should be addressed: Dept. of Biochemistry, 347 Medical Science Bldg., University of Alberta, Edmonton, Alberta T6G 2H7, Canada. Tel.: 780-492-1848; Fax: 780-492-0886; E-mail: lfliegel@ualberta.ca.

is a smaller family that mediates transmembrane export of one to two Na^+ ions in exchange for an extracellular H^+ (5).

The mechanism of transport of Na^+/H^+ exchangers is of great interest because of both the potential to improve salt tolerance in plants and make salt-resistant phenotypes and as a fundamental scientific problem. Significant progress has been made in the understanding of bacterial transport by NhaA (6). However, eukaryotic transporters are not as well understood, have a different exchange stoichiometry, and are activated by different physiological conditions. NHE1 is the most well characterized mammalian Na^+/H^+ exchanger, and we have determined the structure and critical residues of several membrane-associated fragments of NHE1 (9–15). One of the critical TM[5] segments is TM IV, which has been compared with the important TM IV of *E. coli* NhaA (14, 16). We have previously examined several key residues of Sod2 in different transmembrane segments of the protein (3, 4, 17, 18). In this study, we examined the structure and function of a transmembrane segment of this yeast salt tolerance protein. Our results demonstrate that TM IV of Sod2 is critical to Sod2 function with amino acids 144–147 comprising part of a region critical for transport. This study is the first structural and functional characterization of an entire transmembrane segment of a yeast salt tolerance membrane protein and demonstrates that this region is critical for cation selectivity and salt tolerance.

EXPERIMENTAL PROCEDURES

Materials—Restriction enzymes were obtained from New England Biolabs (Mississauga, Ontario, Canada). *Pwo* DNA polymerase was obtained from Roche Applied Science.

Strains and Medium—S. pombe bearing the *sod2* gene disruption (*sod2*::*ura4*) was used for all transformations and as a control where indicated (3). It was maintained on low sodium minimal KMA medium or yeast extract adenine using methods described earlier (1, 3). KMA medium was used where indicated and contains 3 g/liter potassium hydrogen phthalate, 3 g/liter K_2HPO_4, 7 g/liter yeast nitrogen base without amino acids, 20 g/liter glucose, and 200 mg/liter adenine. Leucine at 200 mg/liter was added to maintain the *sod2*::*ura4 leu1-32* strain where indicated, and all media were buffered using 50 mM MES, citrate and adjusted to pH 5.0 with KOH. Wherever indicted NaCl or LiCl was added to the medium. For growth curves in liquid medium, 5×10^6 cells from an overnight exponentially growing culture were inoculated into 2.5 ml of fresh liquid medium. *S. pombe* containing the pREP-41Sod2GFP plasmid (and mutant derivatives) were routinely grown in medium in the absence of thiamine. Cultures were grown at 30 °C with constant agitation using a rotary shaker. The A_{600} was determined at the various times indicated. Growth curves were determined a minimum of three times, and results are mean ± S.E. The plasmid pREP-41Sod2GFP was used for Sod2 expression and has been described earlier (19). pREP-41Sod2GFP contains the entire *sod2* gene plus a C-terminal GFP tag separated by a nine-amino acid Gly-Ala spacer. The GFP has the S65T mutation, and an NdeI site was removed by silent mutation to assist in cloning. In one set of experiments, we compared growth of GFP-fused Sod2 with that of non-GFP-fused Sod2 described earlier (3).

Growth on plates was supplemented with NaCl or LiCl at the indicated concentrations in KMA medium with leucine agar. The plasmid pREP-41Sod2GFP without any mutations (19) was used as a control.

Sod2 TM IV (see below) was expressed in XL1-Blue cells as a maltose-binding protein fusion using a modified pMal-c2X containing a tobacco etch virus (TEV) protease cleavage site between maltose-binding protein and the peptide of interest. Expression was induced with isopropyl 1-thio-β-D-galactopyranoside in either LB (for unlabeled peptide) or M9 (for labeled samples) medium. Expression was initially optimized as follows: for LB medium, 0.6 mM isopropyl 1-thio-β-D-galactopyranoside, 37 °C, 24 h; for M9 medium, 1 mM isopropyl 1-thio-β-D-galactopyranoside, 22 °C, 48 h. LB medium contains 1% (w/v) tryptone, 0.5% (w/v) yeast extract, and 1% (w/v) NaCl. M9 medium contains 7.5 mM $(^{15}NH_4)_2SO_4$, 28 mM glucose, 30 μM thiamine, [47 mM Na_2HPO_4, 22 mM KH_2PO_4, 8.5 mM NaCl], [30 μM $MnSO_4 \cdot 1H_2O$, 3.3 μM $FeSO_4 \cdot 7H_2O$, 203 μM $MgSO_4 \cdot 7H_2O$, 3.4 μM $CaCl_2 \cdot 2H_2O$], and [60 mM K_2HPO_4, 36 mM KH_2PO_4, pH adjusted to 7.5 with KOH] where the individual components or mixtures contained within the square brackets were autoclaved separately and combined afterward.

Site-directed Mutagenesis—Mutations to Sod2 were made to the pREP-41Sod2GFP plasmid directly. The mutations created or removed a restriction enzyme site as described earlier (20). Supplemental Table 1 summarizes the mutations made to the *sod2* gene. DNA sequencing was used to confirm the accuracy of the mutations and fidelity of DNA amplification.

Western Blotting of Sod2—Western blot analysis was used to compare levels of Sod2 expression (20). Cell lysates were made from 50-ml cultures of yeast transformed with wild type and mutant pREP-41Sod2GFP. Yeast cells grown in KMA medium to an A_{600} of 2 at 30 °C. Cells were pelleted (3500 × *g*, 10 min), washed with double distilled water, and resuspended in lysis buffer (50 mM Tris-HCl, pH 8.0, 5 mM EDTA, protease inhibitor mixture (21), and 1 mM dithiothreitol). Cells were then lysed using a Bullet Blender® using 0.5-mm zirconium oxide beads at a speed of 10 for 40 min. In some cases, they were passed through an EmulsiFlex homogenizer at a pressure of 25,000 p.s.i. Unbroken cells were pelleted by centrifugation at 3500 × *g* for 5 min, and the supernatant was centrifuged at 14,000 × *g* for 10 min. Enriched membranes of the supernatant were then pelleted at 100,000 × *g* for 1 h and resuspended in a small volume of the same buffer. Equal amounts of up to 25 μg of each sample were resolved on a 10% SDS-polyacrylamide gel. Nitrocellulose transfers were immunostained using the primary antibody anti-GFP polyclonal antibody (a generous gift from Dr. Luc Berthiaume, Department of Cell Biology, University of Alberta). The secondary antibody was IRDye 680-conjugated goat anti-rabbit polyclonal antibody (Bio/Can, Mississauga, Ontario, Canada). The Odyssey scanning system was used for Western detection (LI-COR Biosciences). Immediately after transfer and prior to immunostaining, nitrocellulose transfers

[5] The abbreviations used are: TM, transmembrane; TM IV, transmembrane segment IV; TEV, tobacco etch virus; MBP, maltose-binding protein; HSQC, heteronuclear single quantum correlation.

were stained with Ponceau S to ensure equivalent loading and transfer of samples (22).

Trypsin Treatment of Microsomal Membranes—Yeast cell membranes were prepared as described above and were made to a concentration of 2 mg/ml in 1 mM EDTA adjusted to pH 7.4 with Tris-HCl. Trypsin (tosylphenylalanyl chloromethyl ketone-treated trypsin; Sigma) was added to give a trypsin:protein ratio of 1:200 and incubated at 30 °C for the times indicated. The reaction was terminated by the addition of SDS-PAGE sample buffer, and samples were resolved on 12% SDS-polyacrylamide gels. Western blotting against the GFP tag was performed to examine protein fragmentation (4). Western blot bands were quantified using ImageQuant TL software (GE Healthcare).

Microscopy and Indirect Immunofluorescence—Confocal imaging of *S. pombe* containing GFP-tagged Sod2 was performed on an Olympus IX81 microscope equipped with a Nipkow spinning disk optimized by Quorum Technologies (Guelph, Ontario, Canada). Images were acquired with the 60× objective on a Hamamatsu EM-CCD camera (Hamamatsu, Japan) using the software Volocity (Improvision Inc., Lexington, MA). Either yeast cells were fixed in 4% formaldehyde prior to imaging, or for live cell imaging, confocal microscopy was used to examine the GFP tag on Sod2 essentially as described earlier (19).

Indirect immunofluorescence was performed using an antibody cross-reactive to the plasma membrane H^+-ATPase of *S. pombe* and originally made against *Neurospora* H^+-ATPase (a generous gift from Dr. C. Slayman, Yale School of Medicine). Cells were prepared for immunofluorescence by treatment with Zymolyase essentially as described earlier (23). Cells were labeled with rabbit anti-H^+-ATPase antibody at a dilution of 1:1000. Visualization was with Cy3-conjugated donkey anti-rabbit antibody (Jackson ImmunoResearch Laboratories, West Grove PA) at a dilution of 1:250.

Atomic Absorption Spectrophotometry—To determine the ability of wild type and mutant Sod2 proteins to remove intracellular Na^+ or Li^+, various strains were grown in KMA medium to an A_{600} of ~0.4. Cells were harvested by centrifugation, washed, and then incubated in KMA medium supplemented with either 100 mM NaCl or 10 mM LiCl for 1 h to load the cells with the appropriate cation. Cells were then harvested; washed two times with 20 mM MES, pH 7.0; and resuspended in 10 ml of buffer containing 20 mM MES, pH 5.5, 0.1 mM $MgCl_2$, and 2% glucose at 30 °C. Samples were taken at various intervals up to 2 h, and Na^+ or Li^+ content was determined by atomic absorption spectrophotometry as described earlier (4). Results from at least three independent experiments are shown.

Sod2 TM IV Peptide Purification—Amino acids 125–154 (LFPQINFLGSLLIAGCITSTDPVLSALIVG) of Sod2 were expressed as a fusion protein with maltose-binding protein. The design was such that we also introduced three additional N- and C-terminal lysines to the peptide. This was done to aid solubilization of the peptide as described earlier (13, 15). The primers SodMBPf (5′-CATGGGATCCAAAAAAAAATTGTTTCCACAAATTAACTTTTTAGG-3′) and SodMBPr (5′-CCGGGAATTCTCATTTCTTTTTTCCTACAATCAATGCTGATAG-3′) were used to amplify the DNA of *sod2* and add the terminal lysines. The primers were designed to allow for in-frame expression with MBP in a modified pMal-c2X plasmid (24), which also has a TEV protease site upstream of the insert to allow for cleavage from the MBP. PCR was performed using the pREP-41Sod2GFP plasmid as a template. The PCR product contained the TM IV sequence with the modified termini flanked by a 5′ BamHI restriction endonuclease site and a 3′ EcoRI site. After cloning into the modified pMal-c2X vector mentioned above, the plasmid construction was confirmed by DNA sequencing.

The *E. coli* strain XL1-Blue was used for expression. Expression and purification were similar to the procedures used by Douglas *et al.* (24). After induction, cells were pelleted by centrifugation at 4000 × *g* and stored at −20 °C. For purification, cell pellets were suspended at ~0.3 g/ml of purification buffer containing 10 mM sodium phosphate buffer, pH 7, 60 mM NaCl, 0.5 mM EDTA, 20% (v/v) glycerol, 0.02% NaN_3 plus added HALT protease inhibitor mixture (EDTA-free) (Thermo Scientific, Rockford, IL)/liter. The cells were lysed using either ultrasonication (Branson sonifier, Emerson Industrial Automation, Danbury, CT) or high pressure homogenization (EmulsiFlex-C3, Avestin Inc., Ottawa, Canada). Samples were then clarified by centrifugation at 50,000 × *g* for 30 min at 4 °C. The supernatant containing MBP-Sod2 fusion protein was loaded onto an amylose affinity column (New England Biolabs, Mississauga, Ontario, Canada) and allowed to incubate with agitation for 1–2 h at 4 °C. The resin was washed with 3 column volumes of cold purification buffer, and the fusion protein was eluted in cold elution buffer (purification buffer + 60 mM maltose). For efficient cleavage of the maltose-binding protein tag, the eluent was concentrated to >5 mg/ml, and 1 mM DTT was added. The Sod2 fragment was cleaved free of the MBP using TEV protease at 10 units/mg of fusion protein for 48–72 h at 16 °C. The protein was then precipitated by the addition of trichloroacetic acid (1.5 g/100 mg of fusion protein) and pelleted by centrifugation. After brief washes with water to remove residual TCA, the pellet was subjected to liquid-liquid extraction with $CHCl_3$: 2-propanol:water (5:5:1 ratio). First the organic solvents were mixed and added to the pellet. Gentle scraping was used to break the pellet up into small pieces before homogenization with a glass Dounce homogenizer. After most of the pellet was pulverized, the appropriate amount of water was added to the homogenizer, and homogenization continued. When the remaining insoluble material appeared quite "fibrous," the mixture was added into a separatory funnel, shaken intermittently throughout the day, and then left to separate overnight. In the morning, the organic (bottom) layer was removed and put in a clean separatory funnel. One volume of fresh water was added, and the extraction was repeated. The resulting organic layer was then used directly for NMR studies. Most complete extraction of the hydrophobic peptide was achieved at 1 ml = 1 volume/30 mg of fusion protein (*i.e.* 5 ml of $CHCl_3$, 5 ml of 2-propanol, and 1 ml of water/30 mg of fusion protein. For studies of unlabeled peptide, deuterated solvents (Cambridge Isotope Laboratories, Andover, MA) were used, and the extraction was carried out at higher protein concentrations (*i.e.* 1 volume/100 mg of fusion protein). For ^{15}N-labeled samples, $CDCl_3$ and undeuterated 2-propanol were used. The identity of the puri-

fied peptide was confirmed by MALDI-TOF mass spectrometry. The purity of the Sod2 TM IV peptide was estimated at over 95%.

NMR Spectroscopy—Peptide samples obtained from liquid-liquid extraction were used for high resolution NMR spectroscopy. After testing with various membrane mimetics, examination of one-dimensional ^{1}H NMR and two-dimensional ^{15}N HSQC NMR spectra indicated that the best solvent system for Sod2 TM IV was $CDCl_3$/isopropanol-d_8. By drying the organic extract under a gentle stream of nitrogen gas, a sample adequately concentrated for structure determination was obtained. $CDCl_3$ in the extract was used as a lock solvent, and spectra were referenced to tetramethylsilane added to the solvent.

All NMR spectra were acquired at 500 MHz and 30 °C. Two-dimensional ^{15}N HSQC (25), three-dimensional ^{15}N NOESY-HSQC (150-ms mixing time) (26), total correlation spectroscopy-HSQC (50-ms mixing time) (26), and HNHA (27, 28) spectra were collected with VnmrJ (Varian Inc.) and processed in NMRPipe (29). Resonance assignment and analysis were performed in NMRViewJ (30). Xplor-NIH (31) was used to model the secondary structure of the peptide.

Homology Modeling—A homology model of Sod2 was created with the program Modeller (32) using the crystal structure of *E. coli* NhaA (Protein Data Base code 1ZCD). *Arabidopsis thaliana* SOS1 was used as a mediator to align Sod2 and NhaA using Clustal Omega (33) on the European Molecular Biology Laboratory-European Bioinformatics Institute server (34). The alignment was refined by using the TMHMM2 secondary structure prediction algorithm (35) to predict the location of α-helical transmembrane segments, and the JPred3 algorithm (36) was used to further support the regions of predicted α-helical secondary structure in Sod2. These data, along with the known position of transmembrane helices in NhaA, were used to adjust the alignment to best reflect the most likely position of transmembrane segments in Sod2. Short helical restraints ($\leq$10 residues) in regions where longer helices were predicted were given to Modeller. The validity of the model was analyzed using a protein validation software suite (37) and the ConSurf method (38, 39) on the online server (40).

RESULTS

We examined amino acids thought to be important in activity of a transmembrane segment of the yeast *S. pombe* salt tolerance protein Sod2. Although the transmembrane segment assignments are not certain, amino acids 126–151 were assigned as TM IV based on a previously published (41) model of the protein (supplemental Fig. 1A) based on hydrophobicity analysis. This segment (FPQINFLGSLLIAGCITSTDPVLSAL) mainly comprises very hydrophobic residues with a few polar residues interspersed (supplemental Fig. 1B). The borders of the membrane lipid interface are not known, although for purposes of mutational analysis, 26 amino acids were chosen; this is larger than required for a typical α-helical transmembrane segment to cross a lipid bilayer.

We compared the amino acid sequence of Sod2 with several other related Na^+/H^+ exchanger proteins using the program Clustal Omega (33) (multiple sequence alignment tool from the European Molecular Biology Laboratory-European Bioinformatics Institute (34)). Sod2 did not align well directly with the sequences of human NHE1 or *E. coli* NhaA, although isolated regions did show some similarity (not shown). When Sod2 was compared with a more closely associated salt tolerance protein, SOS1 (42) (Fig. 1*A*), there were significant areas of identity and similarity especially in the sequence proposed to be TM IV. In turn, the TM IV region of SOS1 aligned well with TM VI of NHE1, permitting a three-way alignment of these TM regions of Sod2, SOS1, and NHE1 (Fig. 1*B*). We have recently (15) shown that TM VI of NHE1, rather than TM IV, is structurally related to TM IV of NhaA, which may account for this finding (see "Discussion").

Because Sod2 is the major salt exporter of *S. pombe* (19), initial experiments measured the ability of Sod2 TM IV mutants to rescue salt tolerance in the salt-sensitive *sod2*::*ura4* deletion strain. As both LiCl and NaCl are transported by Sod2 (3), we examined the ability of mutant proteins to rescue growth in LiCl- or NaCl-containing medium. Aside from NaCl challenge, LiCl was used for assays in liquid and solid media. LiCl is toxic at lower concentrations than NaCl, avoiding osmotic challenge that might occur with the use of high concentrations of NaCl. Figs. 2 and 3 and supplemental Figs. 2 and 3 illustrate the effect of mutations of TM IV on the ability to restore salt tolerance in liquid medium (summarized in Table 1). Fig. 2 and supplemental Fig. 2 demonstrate that the *sod2*::*ura4* strain is intolerant to LiCl concentrations of 5 and 10 mM. In contrast, *S. pombe* with wild type Sod2 protein grows well in LiCl concentrations up to 10 mM with only a slight reduction in growth compared with growth in 0 mM LiCl. The presence or absence of the GFP tag did not affect resistance to growth in LiCl or NaCl (supplemental Figs. 2E and 3E). Supplemental Figs. 4 and 5 illustrate complementary experiments in solid medium. *S. pombe* containing wild type Sod2 was able to grow on solid medium containing up to 10 mM LiCl, whereas the *sod2*::*ura4* knock-out showed reduced growth in 5 mM LiCl and almost no growth in 10 mM LiCl.

A variety of categories of effects was obtained with mutation of TM IV, and the mutants were divided into groups according to their characteristics (Table 1). Results are shown in Figs. 2 and 3 and supplemental Figs. 2–5. Group I mutants showed no effect of the mutation in either liquid or solid medium. This group included F126A, P127A, Q128A, I129A, F131A, I137A, C140A, I141A, T142A, S143A, L148A, and L151A. Group II mutants had very mild effects on growth in either liquid medium, solid medium, or both. For example, in some cases, they showed good salt tolerance in liquid in the presence of 5 mM LiCl but slightly reduced growth with 10 mM LiCl. This group included N130A, L132A, G133A, S134A, L135A, L136A, G139A, S149A, L151S, and I152A. Group III mutants had a very marked effect on both NaCl and LiCl tolerance in both solid and liquid media. This group included T144A, T144D, T144K, V147A, and V147L. Groups IV and V were unique categories consisting of one mutant. Group IV contained T144S, which was inactive or nearly so in NaCl-containing medium but functional in LiCl-containing medium. This was notable because other mutations of the same amino acid to either Ala, Asp, or Lys created a nearly non-functional protein. Group V contained

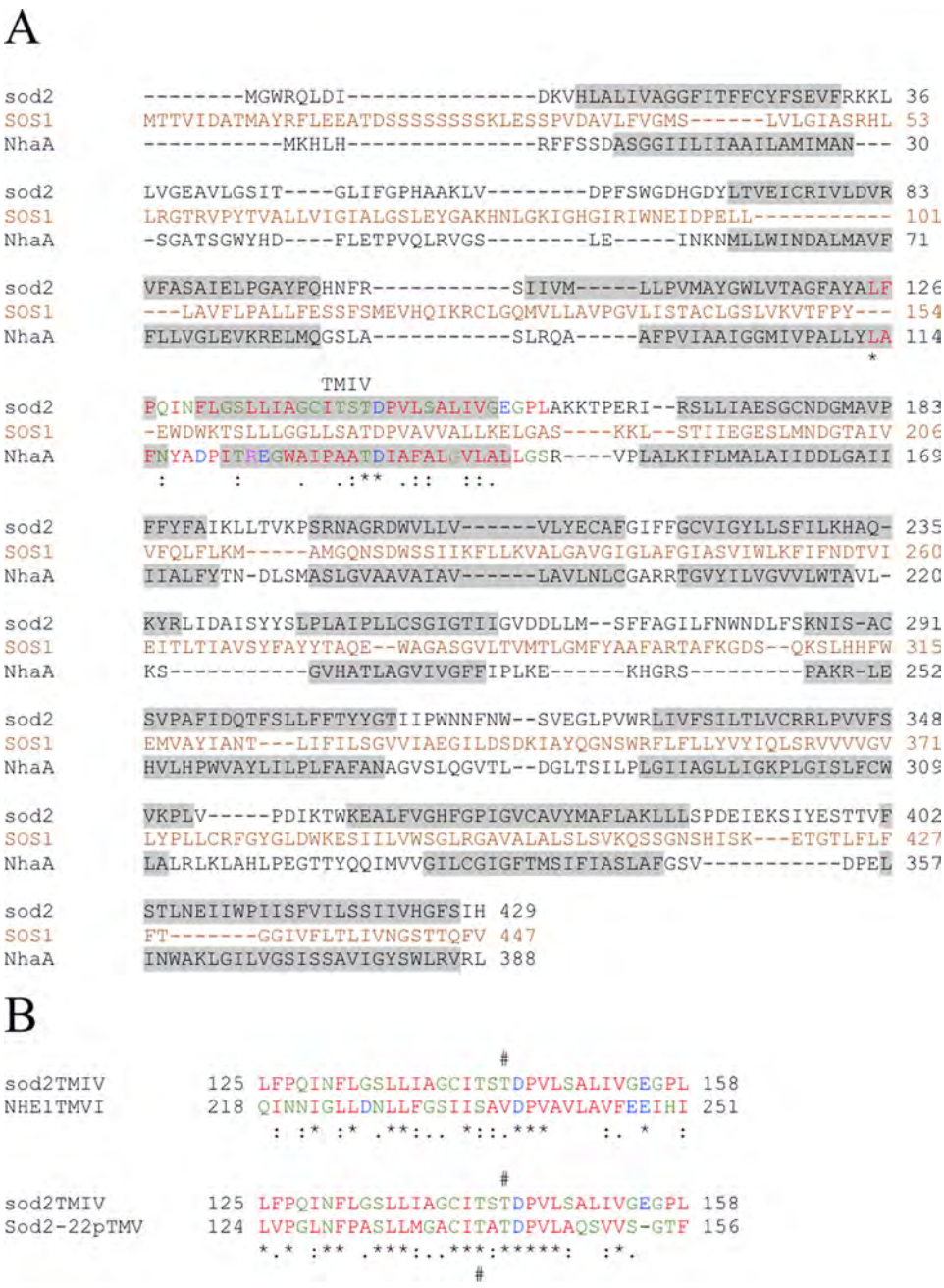

FIGURE 1. *A*, alignment of Sod2 with NhaA using SOS1 as an intermediate as described under "Experimental Procedures." Sod2 TM IV and aligned residues in NhaA are colored (*red*, hydrophobic; *blue*, acidic; *green*, polar; *magenta*, basic) and labeled with Gonnet percent accepted mutation 250 amino acid conservation scores between Sod2 and NhaA TM IV (*, identical; :, strongly similar; .,weakly similar). The transmembrane segments from the crystal structure or the homology model of NhaA and Sod2, respectively, are shaded in *gray*. *B*, sequence alignments of Sod2 TM IV with putative analogous transmembrane segment from human NHE1 (TM VI) and *Zr*Sod2-22p (TM V) colored and labeled as in *C*. The critical threonine residues of Sod2, *Zr*Sod2-22p, and NhaA are denoted by #.

I152A, which had an intermediate phenotype affected partially in both liquid and solid medium and more so in liquid medium with LiCl.

Western blot analysis was used to determine whether all the mutant proteins were expressed. Supplemental Fig. 6 demonstrates that the Sod2-GFP fusion protein was present as a band of ~60 kDa. All mutant proteins were expressed. Ponceau S staining was used to confirm sample transfer after immunoblotting. In some cases, there was evidence of lower molecular weight immunoreactive species. The occurrence of these lower molecular weight species was variable from cell lysate to lysate (not shown), possibly indicating that these were degradation products produced during sample preparation.

To determine whether the mutant Sod2 protein was properly folded, we carried out limited digestion with trypsin. This method examines the proteolytic attack on accessible Arg and Lys and has been used earlier to examine changes in the structure of Sod2 (4) and the mammalian Na^+/H^+ exchanger (43). We compared the digestion of wild type Sod2 with that of the V147A, T144A, and T144S mutants (Fig. 4). We found that the T144A mutant Sod2 protein was digested more rapidly than the wild type with the T144S and the V147A showing intermediate patterns of digestion.

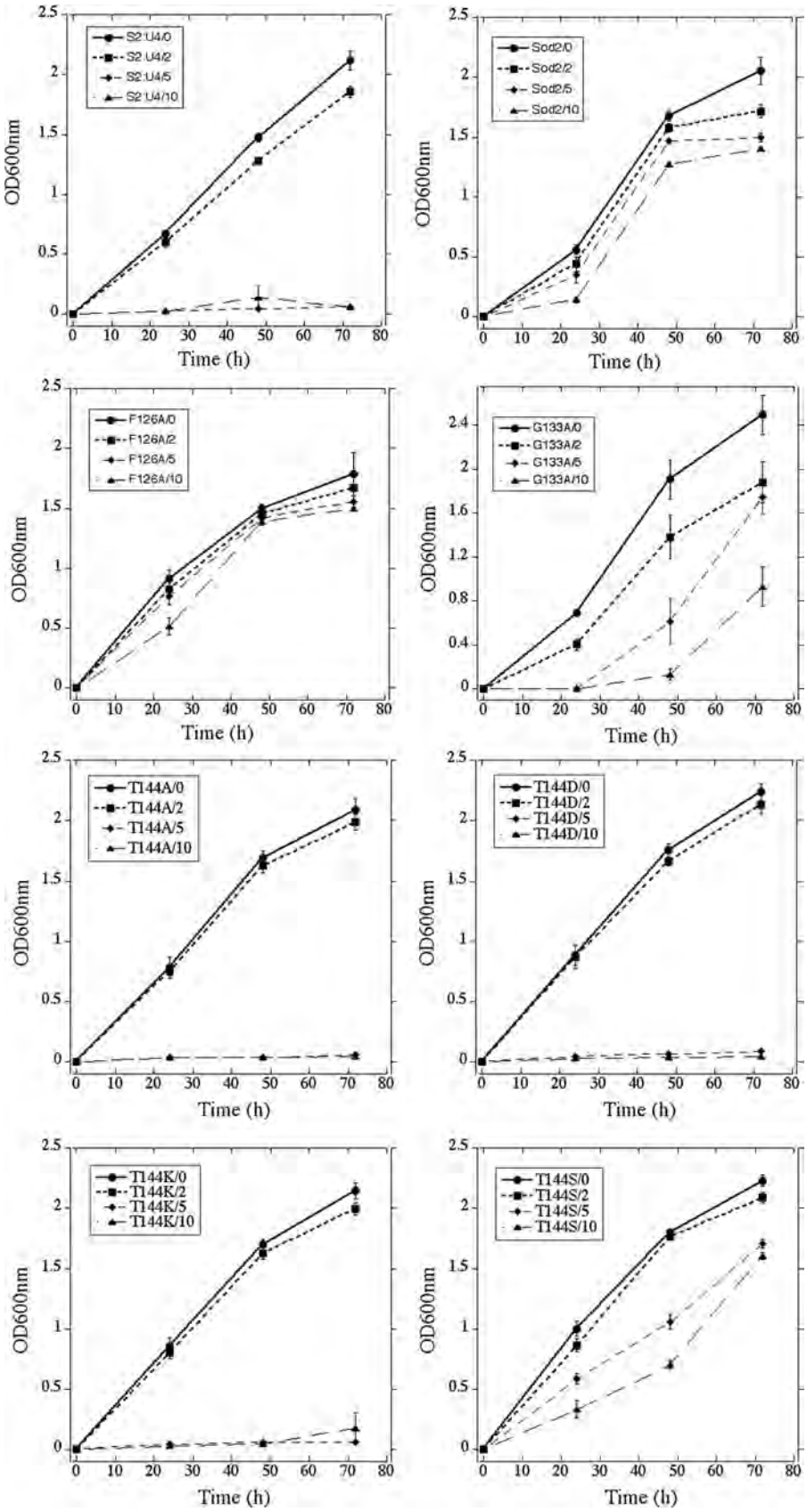
S2:U4/0
S2:U4/2
S2:U4/5
S2:U4/10
Sod2/0
Sod2/2
Sod2/5
Sod2/10
F126A/0
F126A/2
F126A/5
F126A/10
G133A/0
G133A/2
G133A/5
G133A/10
T144A/0
T144A/2
T144A/5
T144A/10
T144D/0
T144D/2
T144D/5
T144D/10
T144K/0
T144K/2
T144K/5
T144K/10
T144S/0
T144S/2
T144S/5
T144S/10
OD600nm
Time (h)

Because we found that mutation of Thr^{144} and Val^{147} was detrimental to the ability of Sod2 to restore growth in salt-containing medium, we further examined the subcellular location of the mutant proteins in *S. pombe* by confocal microscopy (Fig. 5). The H^+-ATPase was used as a plasma membrane marker (Fig. 5*A*). Wild type Sod2-GFP had an irregular distribution, partially on the plasma membrane and partially intracellular, similar to what we have noted earlier (4, 19). The H^+-ATPase was primarily located on the plasma membrane with occasional indications of intracellular labeling possibly due to biosynthesis of the protein. Both T144A and V147A Sod2 mutants were distributed in a manner similar to that of the wild type Sod2. There was evidence of some co-localization on the plasma membrane, and although this was not complete, there were no differences apparent between the wild type Sod2 protein and the mutant proteins. We confirmed the observations on the localization of wild type and mutant Sod2 using live cell imaging (Fig. 5*B*). All mutants and wild type Sod2 had a predominantly plasma membrane localization. Similar to our earlier observations (4), the distribution throughout the membrane was not even with occasional concentration at the apical tips of the membrane.

To gain further insight into the effects of the critical mutations on ion flux in *S. pombe*, we examined the expulsion of intracellular Na^+ and Li^+ as an indication of Sod2 activity. It was demonstrated previously (1, 44) that Sod2 accounts for most of the Na^+ and Li^+ expulsion in *S. pombe*, and its deletion or inactivity results in greatly reduced expulsion of these ions from the cytosol. We examined the decreasing content of these cations after a period of cation loading (4). The results are shown in Fig. 6, *A* and *B*. After incubation in NaCl-containing medium, NaCl content of *S. pombe* expressing wild type Sod2 declined relatively rapidly. In contrast, the *sod2* knock-out and the mutants T144A, T144S, and V147A were all greatly impaired in their ability to reduce cellular Na^+ content (Fig. 6*A*). The mutants were also all impaired in their ability to extrude Li^+ (Fig. 6*B*) with the exception of the T144S mutant, which reduced cellular Li^+ content approximately as well as the wild type Sod2 protein. The V147A mutant also had a slight tendency toward decreasing cellular Li^+ content.

To gain molecular insights into how these functionally important residues may be arranged in the structure of Sod2, we expressed and purified a peptide representing TM IV (GSKKK^{125}LFPQINFLGSLLIAGCITSTDPVLSALIVG^{154}KKK) for NMR experiments. Following purification of a maltose-binding protein fusion protein and cleavage with TEV, an organic liquid extraction technique was used to isolate the hydrophobic TM IV peptide from any remaining aqueous contaminants (Fig. 7). After two rounds of extraction, the organic layer contained relatively pure peptide with only trace amounts of contaminants remaining, and we proceeded directly with NMR experiments using the sample in organic solvent.

Initially, one-dimensional ^1H and then two-dimensional ^{15}N HSQC spectra were used to judge the quality of peptide samples for structure determination while varying the solvent/detergent, pH, and temperature. The peptide was poorly soluble in a $CHCl_3$/MeOH/H_2O mixture, which has been used successfully in previous work for a transmembrane segment of the mammalian Na^+/H^+ exchanger (16). It was also poorly soluble in trifluoroethanol/H_2O, and although the peptide could be solubilized in dodecylphosphocholine, SDS, or DMSO, these samples only gave moderate quality two-dimensional ^{15}N HSQC spectra (Fig. 8*A*). The peaks were broader and less well resolved than a sample in $CHCl_3$/isopropanol. The best spectra were obtained in the solvent mixture used for the organic extraction, $CHCl_3$/isopropanol, and this solvent mixture was used for further NMR analysis. The one-dimensional spectrum showed good dispersion of the backbone amide peaks; however, there was an additional broad intensity underneath the amide region that may have been peptide aggregates or impurities. Peaks were well resolved in a two-dimensional ^{15}N HSQC spectrum, suggesting that the solvent mixture would be suitable for further experiments (Fig. 8*B*). With the exception of proline residues and the N-terminal glycine, complete backbone resonances and partial side chain resonance assignments were obtained from the three-dimensional NMR spectra. A labeled two-dimensional HSQC spectrum is shown in Fig. 8*B*. A few additional peaks were present in the HSQC spectrum that could not be assigned that could result from impurities in the sample or minor conformations from cis-trans isomerization from one or both prolines in the TM IV peptide.

A comparison of the Hα chemical shifts with random coil chemical shifts (supplemental Fig. 7) (45) suggests that there are two α-helical regions: residues 128–142 form a longer helix on the N-terminal half of the peptide, and residues 147–153 form a shorter helix on the C-terminal half. The residues between the helices, 143–146, have shifts close to random coil values and are likely dynamic or extended in structure. The termini are also likely unstructured with Hα shifts close to random coil. The chemical shift data are supported by the $^3J_{HNH\alpha}$ coupling constants as the helical regions have coupling constants around 4–6 Hz, consistent with helical structure, and termini with coupling constants at around 7 Hz, indicating dynamic or unstructured residues. Critical residue Thr^{144} has a coupling constant of about 8 Hz, suggesting that this region between the two helices is adopting an extended conformation. Values for some residues were not determined because of overlap of peaks in the HN region of the spectrum. Proton-proton distances from NOESY data also support the secondary structure prediction (supplemental Fig. 8). Hα-HN (i, i + 3) and

FIGURE 2. **Growth of *S. pombe* containing either wild type or TM IV mutant Sod2 proteins in liquid medium with various concentrations of LiCl.** Examples of growth of *S. pombe* containing no Sod2 (*sod2*::*ura4*), wild type Sod2, a mutated Sod2 with an intermediate phenotype, and a series of Thr^{144} mutants are shown. (All mutants grown in LiCl are shown in supplemental Fig. 2 and summarized in supplemental Table 1.) LiCl tolerance of strains was assessed by inoculating 2×10^6 cells into 2.5 ml of medium at 30 °C for up to 72 h. Growth was assessed by measuring the absorbance of the cell suspensions at 600 nm at the indicated times. Results are the mean ± S.E. (*error bars*) of at least three determinations. *S. pombe* was grown in the presence of 0, 2, 5, or 10 mM LiCl. *S2:U4* refers to *sod2*::*ura4* (*S. pombe* with the Sod2 knock-out described earlier (3)). *Sod2* refers to *sod2*::*ura4* containing the wild type Sod2 protein (19). In other cases, the indicated Sod2 TM IV mutant was introduced into the *sod2*::*ura4* strain in the presence of 0, 2, 5, or 10 mM LiCl as indicated.

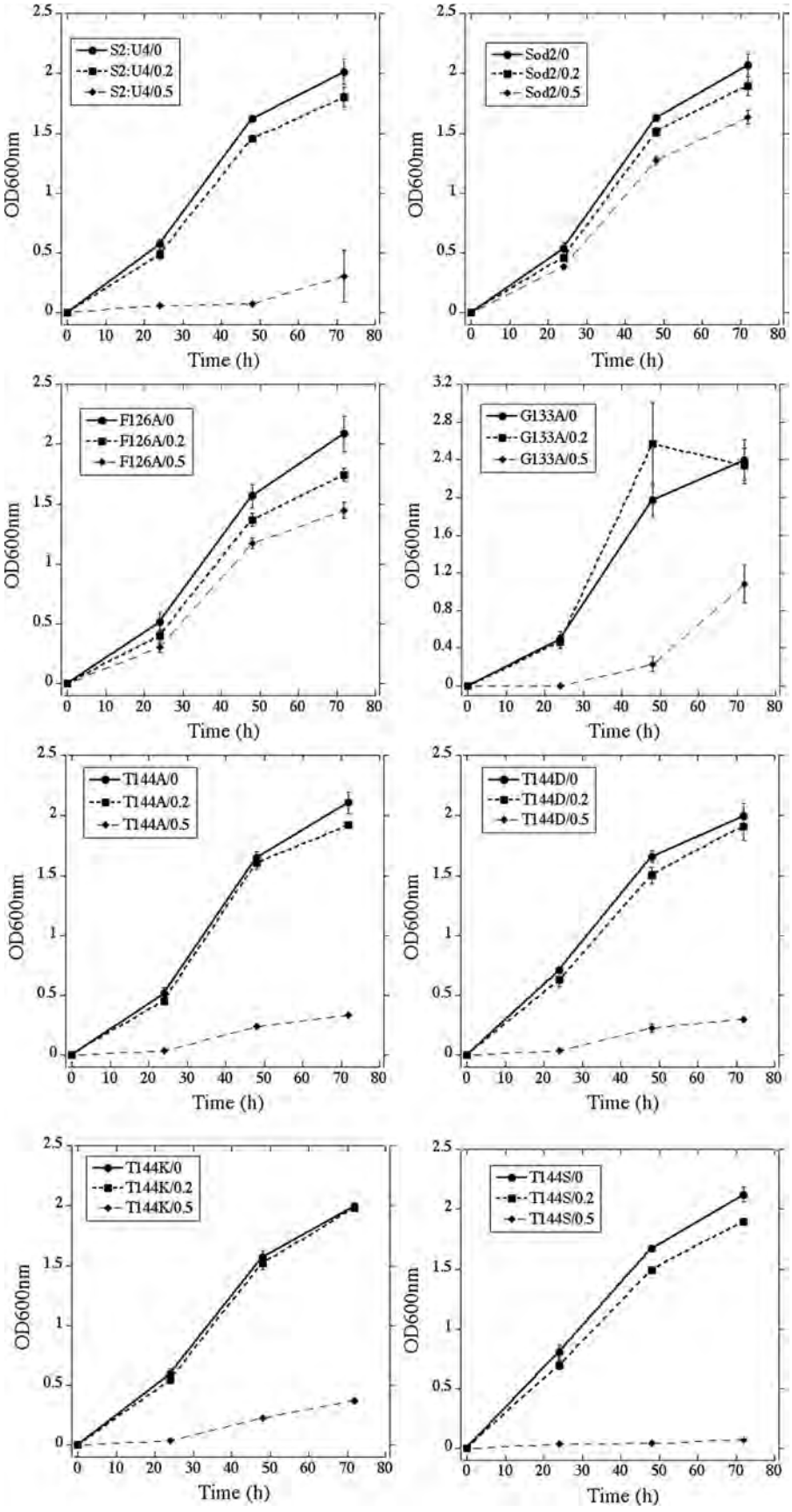
S2:U4/0
S2:U4/0.2
S2:U4/0.5
Sod2/0
Sod2/0.2
Sod2/0.5
F126A/0
F126A/0.2
F126A/0.5
G133A/0
G133A/0.2
G133A/0.5
T144A/0
T144A/0.2
T144A/0.5
T144D/0
T144D/0.2
T144D/0.5
T144K/0
T144K/0.2
T144K/0.5
T144S/0
T144S/0.2
T144S/0.5
OD600nm
Time (h)

TABLE 1

Summary of characteristics of Sod2 TM IV

Effects of mutation of the amino acids and structural characteristics (Str) of the indicated amino acid in deduced NMR structure and structural model are shown. Growth characteristics are indicated as follows: +++, growth essentially equivalent to that supported by wild type Sod2; ++, growth slightly reduced compared with wild type Sod2; +, growth greatly reduced compared with wild type Sod2 but still greater than that of Sod2 knock-out; −, growth essentially equivalent to Sod2 knock-out yeast. Group refers to the following groupings: I, no effect of mutation on salt tolerance; II, very mild effect; III, marked effect on NaCl and LiCl tolerance; IV, marked effect on NaCl tolerance only; and V, intermediate effect on NaCl and LiCl tolerance. D, disordered; E, extended; H, helix; L, loop; N/A, not applicable.

Mutation	Liquid LiCl	Liquid NaCl	Solid LiCl	Solid NaCl	Group	Str NMR	Str model
sod2 WT	+++	+++	+++	+++	N/A		
F126A	+++	+++	+++	+++	I	D	L
P127A	+++	+++	+++	+++	I	D	L
Q128A	+++	++	+++	+++	I	D	L
I129A	+++	+++	++	+++	I	H	L
N130A	+++	+++	++	+++	II	H	L
F131A	+++	+++	+++	+++	I	H	H
L132A	++	++	++	+++	II	H	H
G133A	++	++	++	++	II	H	H
S134A	++	++	++	++	II	H	H
L135A	++	++	++	++	II	H	H
L136A	+++	+++	++	++	II	H	H
I137A	+++	+++	+++	+++	I	H	H
G139A	+++	+++	++	++	II	H	H
C140A	+++	+++	+++	+++	I	H	H
I141A	+++	+++	+++	+++	I	H	H
T142A	+++	+++	+++	+++	I	H	H
S143A	+++	+++	+++	+++	I	E	E
T144A	−	−	+	+	III	E	E
T144D	−	−	+	+	III	E	E
T144K	−	−	+	+	III	E	E
T144S	+++	-	+++	+	IV	E	E
Asp^{145}	N/A	N/A	N/A	N/A	N/A	E	E
Pro^{146}	N/A	N/A	N/A	N/A	N/A	E	H
V147A	−	−	+	+	III	E	H
V147L	−	−	−	−	III	E	H
L148A	+++	+++	+++	+++	I	H	H
S149A	++	+++	+++	+++	II	H	H
L151A	+++	+++	+++	+++	I	H	H
L151S	++	+++	+++	+++	II	H	H
I152A	+	++	++	++	V	H	H

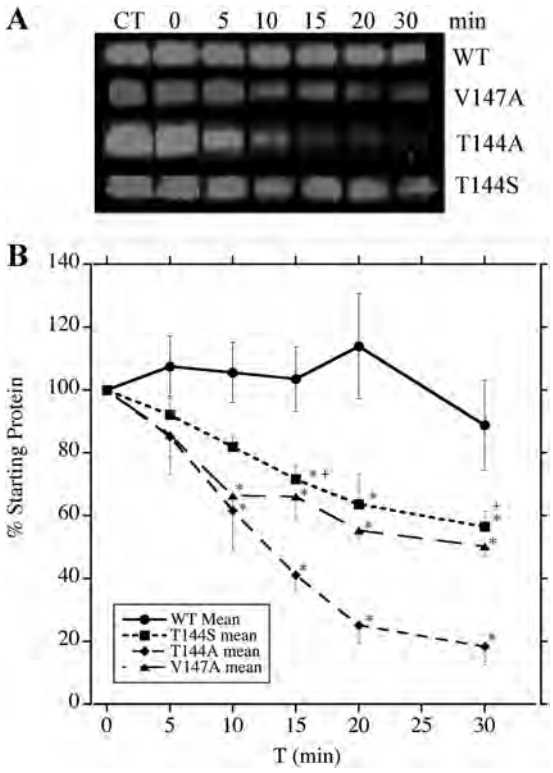

FIGURE 4. **Analysis of susceptibility of mutant and wild type Sod2 protein to trypsinolysis.** Yeast cell membrane fractions were incubated with a 1:200 trypsin:protein ratio for 0–30 min at 30 °C as described under "Experimental Procedures." Samples were then analyzed by SDS-PAGE and Western blotting using anti-GFP antibody. *A*, Western blot of wild type (*WT*) and Sod2 mutant proteins. *B*, summary of effects of trypsin on percentage of Sod2 protein remaining over time. Results are mean ± S.E. (*error bars*) of at least four experiments. *, significantly different from WT at $p < 0.05$; +, significantly different from T144A at $p < 0.05$. *CT*, control.

(i, $i + 4$) contacts can be observed within the two helical regions. Further evidence of the extended region between the two helices is shown by the presence of exchange NOE peaks at 4.8 ppm to the residual water in the sample (supplemental Fig. 9), indicating interactions with water with this region.

A model representing the likely structure that Sod2 TM IV could adopt was constructed with Xplor-NIH (31) using the $^3J_{HNH\alpha}$ and the Hα chemical shift data (Fig. 9). The model structure calculation begins with a simple extended polypeptide upon which the measured NMR restraints are added and energy minimization calculations are performed. This process was followed several times, analyzing violations resulting from conflicts between the data and the model. Residues that had large errors in the calculations or where the $^3J_{HNH\alpha}$ and chemical shift data conflicted or were ambiguous were not included in the modeling. The model displays disordered termini, a longer helical stretch of residues 129–142, an extended region from residues 143 to 147, and a shorter helix from residues 148 to 153. The NMR data and model have been deposited in the Protein Data Bank and Biological Magnetic Resonance Data Bank (Protein Data Bank code 2M7X).

To gain insight into the potential role of TM IV in the folded structure of Sod2 and to provide evidence that the deduced structure of TM IV was correct, we constructed a homology-based model of the entire Sod2 protein. The model was based on the crystal structure of *E. coli* NhaA, the only Na^+/H^+ exchanger with a high resolution crystal structure available. As noted above, Sod2 did not align directly with NhaA using the Clustal Omega alignment program (33). To overcome this problem, we used SOS1 as an alignment template as it aligned with both NhaA and Sod2 (Fig. 1*A*). These alignments were then used to construct a sequence comparison between NhaA and Sod2. The initial model largely resembled the architecture of NhaA except for one large structural anomaly wherein amino acids 237–255 formed a long loop that traversed parallel through the membrane domain, looping around two transmembrane segments. Closer analysis of this feature indicated that several of the residues were in steric conflict and that this structure was invalid. To resolve this, we sought to improve our

FIGURE 3. **Growth of *S. pombe* containing either wild type or TM IV mutant Sod2 proteins in liquid medium with various concentrations of NaCl as described for Fig. 2.** Examples of growth of *S. pombe* containing no Sod2 (*sod2*::*ura4*), wild type Sod2, a mutated Sod2 with an intermediate phenotype, and a series of Thr^{144} mutants are shown. (All mutants grown in NaCl are shown in supplemental Fig. 3 and summarized in supplemental Table 1.) NaCl was added at concentrations of 0, 0.2, or 0.5 M as indicated. Results are the mean ± S.E. (*error bars*) of at least three determinations.

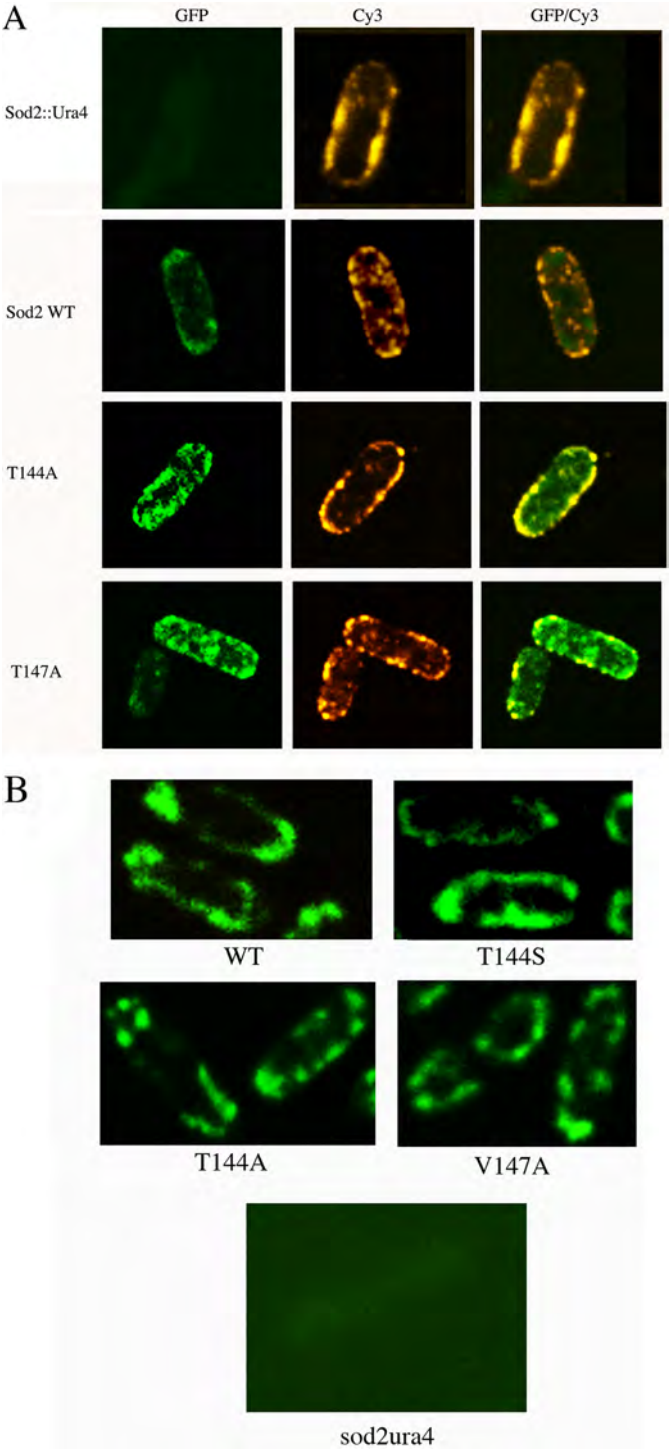

FIGURE 5. **Confocal microscopy of *S. pombe* expressing wild type Sod2-GFP and Sod2-GFP with mutations in TM IV.** *A*, exponentially growing cells were harvested, treated with Zymolyase, washed, and mounted on coverslips before imaging. *Rows* indicate the yeast strain. *sod2::ura4* indicates the *S. pombe* knock-out strain without the Sod2 protein. *Sod2* refers to the wild type Sod2 protein expressed in *S. pombe*. *Rows T144A* and *T147A* indicate Sod2 protein with these point mutations. The *left column* illustrates GFP fluorescence. The *center column* illustrates Cy3 (*red*) fluorescence (H^+-ATPase). The *right column* illustrates both Cy3 and GFP fluorescence. *B*, exponentially grown cells were harvested and used directly for live cell imaging of GFP fluorescence.

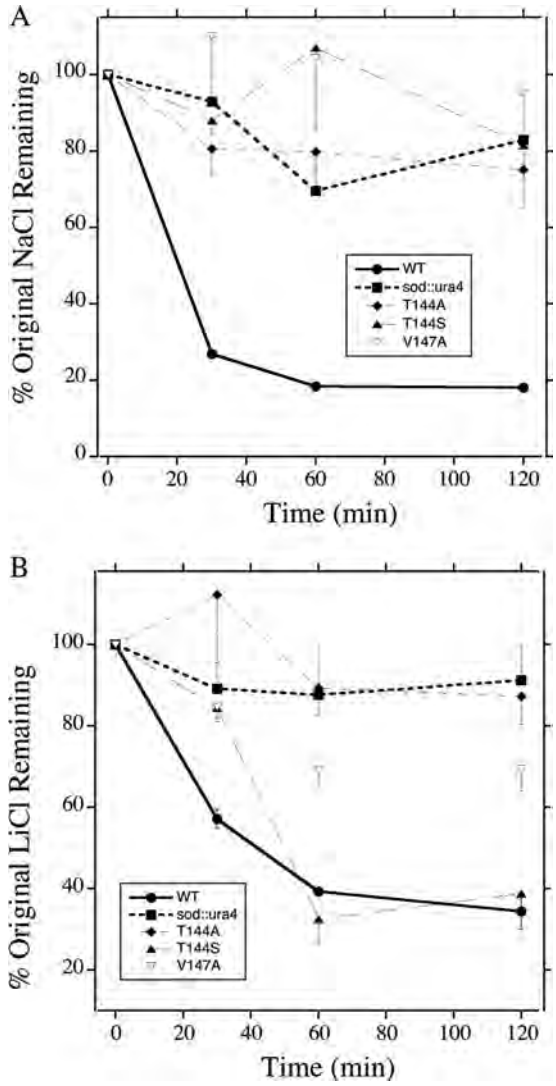

FIGURE 6. **Loss of Na^+ or Li^+ content from *S. pombe* containing wild type or mutant Sod2 proteins.** Cells expressing various indicated Sod2 proteins or the *sod2::ura4* knock-out strain were incubated in high NaCl- (*A*) or LiCl (*B*)-containing medium for 1 h and resuspended in Na^+- or Li^+-free medium. The Na^+ or Li^+ content was determined by atomic absorption spectrophotometry as described under "Experimental Procedures." Results are the mean ± S.E. (*error bars*) of at least three experiments. Where not shown, S.E. was too small to be displayed.

sequence alignment using the TMHMM2 secondary structure prediction algorithm (35) to predict the location of α-helical transmembrane segments in Sod2. Significantly, the predicted helical regions aligned approximately with the actual locations of transmembrane segments in NhaA, giving an unbiased indication that our initial alignment was reasonable. The predictions were further corroborated using the JPred3 secondary structure prediction algorithm (36), which indicated very similar helical regions to TMHMM2. Using these secondary structure predictions, the alignment was adjusted so that predicted helices of Sod2 lined up with the known helices of NhaA. This alignment replaced the aberrant intramembrane loop at residues 237–255 with a transmembrane α-helix that satisfied the steric conflicts. However, closer inspection revealed that up to seven amino acids at the ends of several transmembrane helices dipped back into the membrane. To address this, we looked at the predicted length of transmembrane helices in Sod2 *versus* NhaA and noted that many were longer in Sod2 than NhaA. Because Modeller does not account for significant differences

in transmembrane segment length, short helical restraints were added to the ends of the Sod2 transmembrane segments predicted to be longer than the aligned sequence in NhaA. To ensure no undo bias was added by secondary structure prediction, the same TMHMM2 and JPred3 algorithms (35, 36) were used to predict helical regions of NhaA. The algorithm predicted helices that aligned nearly perfectly (fewer than two residues were different) with the actual location of transmembrane helices in the crystal structure (with the exception of the two short helices, 7 and 8, which were predicted to be one long helix). The resulting model (Fig. 10*A*) no longer appeared to have any structural anomalies and was in good agreement with the NhaA structure (Fig. 10*B*). The validity of the model was confirmed using the protein structure validation software suite (37). This evaluation revealed only seven residues with backbone angles outside of the allowable region of the Ramachandran plot. Six of these residues are located in extramembrane loops where the backbone bonds would be flexible enough to adopt a more preferable angle. The seventh residue, Val^{373}, is located in the unwound region of transmembrane segment XI. To resolve the significance of this disallowed dihedral angle, sculpting was performed using PyMOL (Schrödinger, LLC). Upon relaxation of the region containing Val^{373}, admissible dihedral angles were obtained.

The model was further validated from a bioinformatics standpoint using the ConSurf method (38, 39). Using the ConSurf server (40), 91 protein sequences (of >35% identity and a BLAST score of >300) were selected and aligned with the Sod2 sequence. The server then calculated a Bayesian conservation score (0–9), gave it a corresponding color, and mapped it onto the model of Sod2 (supplemental Fig. 10). Regions of high sequence conservation (pink to purple) are (as expected) found in the core of the transporter, whereas regions of less conserva-

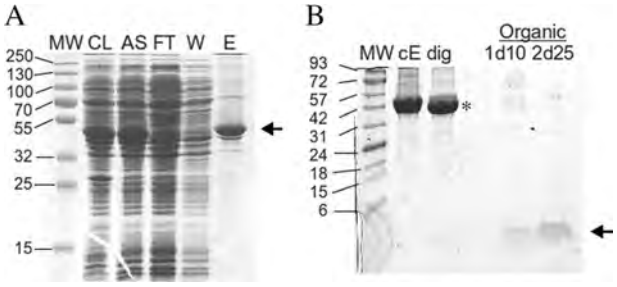

FIGURE 7. **SDS-PAGE (12%) analysis of purification of MBP-Sod2 fusion protein.** *A*, Sod2 TM IV fusion protein was produced and purified as described under "Experimental Procedures," and samples from the purification procedure are illustrated. *CL*, crude bacterial lysate; *AS*, clarified lysate supernatant after ultracentrifugation; *FT*, flow-through, maltose affinity column unbound fraction; *W*, maltose affinity column wash fraction; *E*, maltose affinity column eluted fraction (~2 mg of protein/ml; *MW*, molecular mass ladder (kDa). The *arrow* denotes the position of the fusion protein. *B*, Tris-Tricine (16%) analysis of TEV cleavage of Sod2 fusion protein followed by organic extraction. *cE*, 10× concentrated elution fraction; *dig*, concentrated elution fraction following 3-day cleavage with TEV; *Organic*, samples of the organic layer following extraction; *1d10*, 10 μl of organic layer following one round of extraction; *2d25*, 25-μl sample of organic layer following two rounds of extraction; *MW*, molecular mass ladder (kDa). * denotes the position of the maltose-binding protein after cleavage and removal of Sod2 protein. The *arrow* denotes the position of the Sod2 protein in the organic fraction.

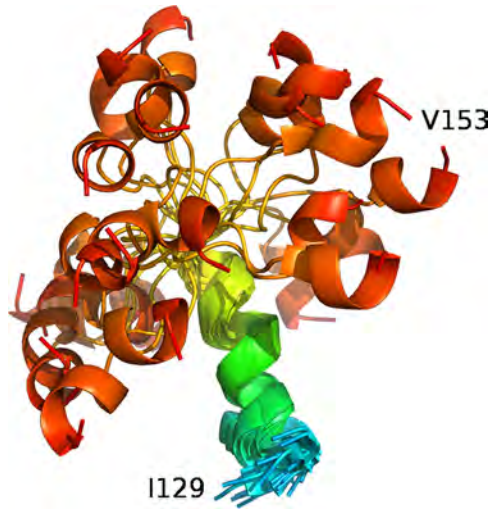

FIGURE 9. **Ensemble of 25 models of Sod2 TM IV created with Xplor-NIH.** Side view of the ensemble with the structures superimposed along the N-terminal helix (Protein Data Bank code 2M7X). Only residues Ile^{129}–Val^{153} are shown for clarity as the amino and carboxyl ends of the structures were disordered.

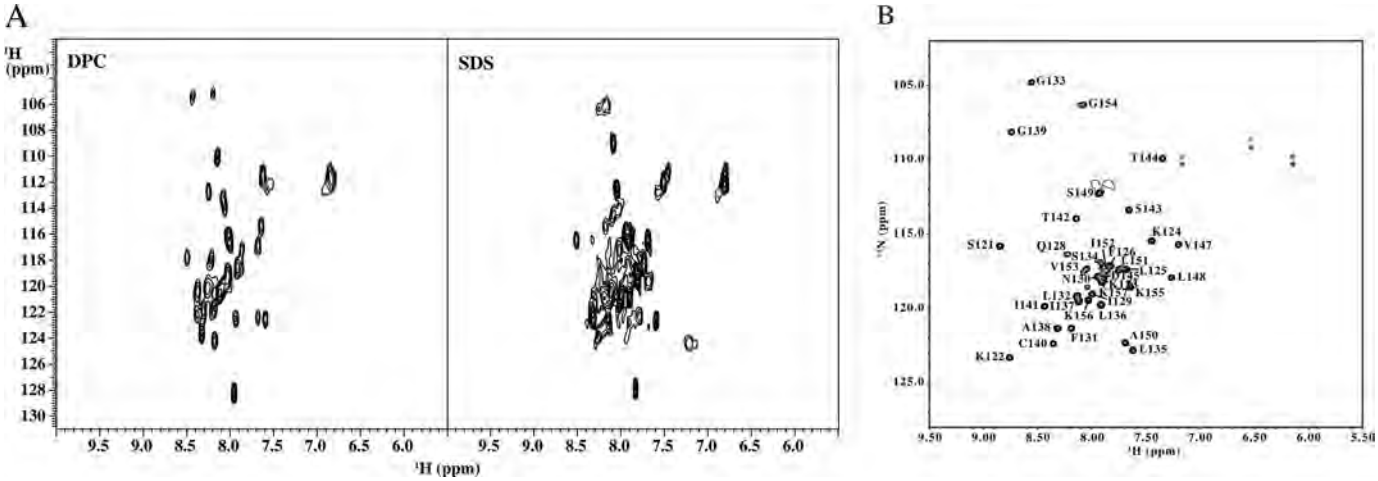

FIGURE 8. **Two-dimensional ^{15}N HSQC spectra of Sod2 TM IV peptide.** *A*, two-dimensional ^{15}N HSQC spectra of Sod2 TM IV peptide in detergent micelles. Samples in detergent micelles were prepared from peptide in organic solvent that was dried under $Ar_{2(g)}$ and reconstituted in 1% dodecylphosphocholine or SDS, 10 mM imidazole, 0.25 mM DSS, 95% H_2O, and 5% D_2O, pH 6.0. Spectra were acquired at 500 MHz and 30 °C. *B*, two-dimensional ^{15}N HSQC of Sod2 TM IV in 50% $CDCl_3$ and 50% isopropanol with assignments indicated. The sample was taken directly from the organic extraction procedure and partially concentrated by slow evaporation under $N_{2(g)}$.

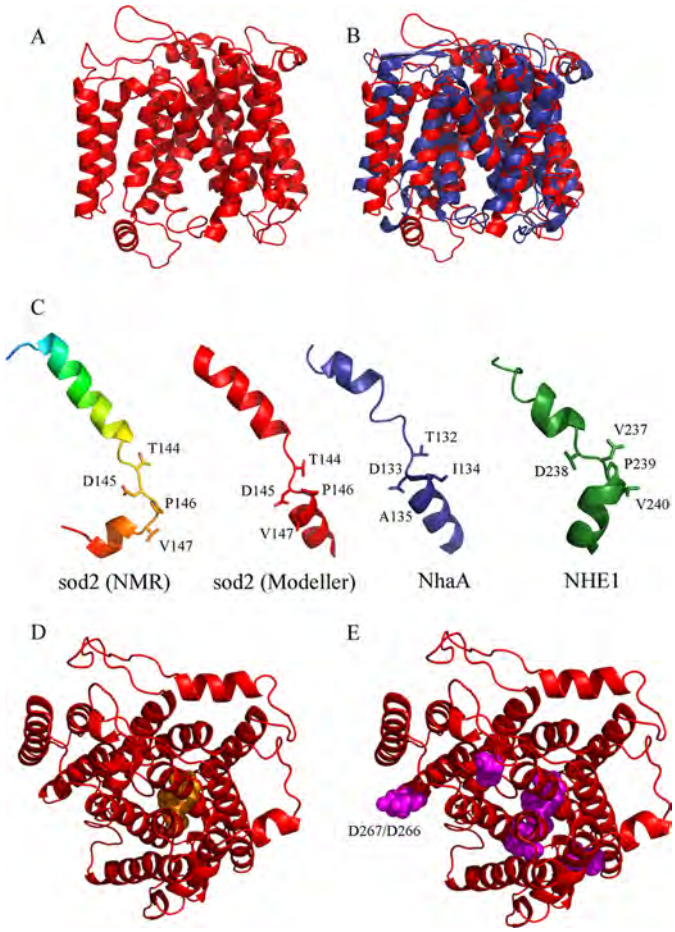

FIGURE 10. **Homology model and TM segment structure comparison.** *A*, homology model of Sod2 membrane domain (residues 12–429) based on the crystal structure of *E. coli* NhaA (Protein Data Bank code 1ZCD) using Modeller software (32). *B*, homology model (*red*) aligned with NhaA (*blue*). *C*, structures of analogous TM segments of NhaA TM IV (*blue*) and NHE1 TM VI (*green*) are shown next to the structural model of Sod2 (NMR) made with Xplor-NIH (*rainbow*) and Sod2 (Modeller) homology model TM IV (*red*). Key residues have been labeled for each peptide (see "Discussion"). *D*, homology model of Sod2 viewed perpendicular to the membrane plane from the extracellular side. The key residues of TM IV (Thr^{144}–Val^{147}) are shown as *orange spheres*. *E*, reproduction of *D* with all known functional mutations indicated in *magenta spheres*. Asp^{266} and Asp^{267} are labeled, indicating their distance from the transport pore.

tion (white to blue) are found on the outer surface. Significantly the critical amino acids ^{144}TDP^{146} all have the highest conservation score of 9, and Val^{147} has a score of 8.

Fig. 10*C* shows a comparison of the deduced and modeled TM segments of Sod2, TM IV and TM IV of NhaA, and TM VI of NHE1. All display a characteristic helix-extended region-helix configuration. The NMR structure of TM IV of Sod2 is very similar, although not identical, to the structure of Sod2 deduced by modeling.

Fig. 10*D* illustrates the homology model of Sod2 viewed perpendicular to the membrane plane from the extracellular side. The key residues of TM IV (Thr^{144}–Val^{147}) are shown as *orange spheres* and have a central, potentially pore-lining location. Fig. 10*E* illustrates the position of all known functional mutations in the model.

DISCUSSION

Removal of excess salt in plants and yeast is crucial in dealing with excess toxic levels of intracellular Na^+. In plants, improvements in salt tolerance have significant agricultural implications for crops. The yeast *S. pombe* is a useful model organism for the study of salt tolerance as the Na^+/H^+ antiporter (Sod2) plays the major role in salt tolerance, and its deletion results in a Na^+- and Li^+-sensitive phenotype (1). Although significant advances have been made in the study of mammalian (46) and *E. coli* (47) Na^+/H^+ exchangers, there has been much less study on plant and yeast Na^+/H^+ exchangers. Here we present the first systematic examination of a transmembrane segment of this type of transporter by alanine scanning mutagenesis and NMR spectroscopy. Alanine scanning mutagenesis was used as described earlier (9, 48). The premise is that the small side chain of alanine can substitute for amino acids without disrupting the protein structure while at the same time altering the nature of the side chain. All the amino acids of TM IV were mutated to alanine except Ala^{138} and Ala^{150} and the earlier characterized Asp^{145} and Pro^{146} (4, 17).

Most of the mutations had either no effect or mild to intermediate effects on the ability of Sod2 to restore salt tolerance in *sod2*::*ura4 S. pombe* (Table 1, Group I and II mutants). However, the effects of mutation of amino acids Thr^{144} and Val^{147} were notable and were explored in more detail. Several experiments suggested that the effects we found on these two amino acids were on cation coordination either directly or indirectly through a change in conformation of the protein. The expression level and localization of these mutant forms of Sod2 were normal. However, limited tryptic digestion suggested that there was a change in conformation of the mutant proteins. This was especially noticeable in the non-functional T144A protein, whereas the conservative substitution T144S was able to transport Li^+ and was not as sensitive to proteolytic digestion. This suggests that the hydroxyl side chain restored not only activity but also a conformational change.

For Thr^{144}, mutation to either Ala, Asp, or Lys did not restore the ability to confer salt tolerance. However, changing Thr^{144} to a serine residue restored the ability to confer resistance to LiCl and to transport LiCl but did not restore NaCl tolerance and transport (Fig. 6). The hydroxyl might be directly participating in the binding of cations. The ionic radii of Na^+ and Li^+ are 0.95 and 0.65 Å, respectively (43). A simple explanation may be that presentation of the hydroxyl by Ser is such that it can coordinate the smaller Li^+ ion but not the larger sodium. Alternatively, it is known that hydrogen bond formation between the side chain oxygen atom of a Ser and Thr and the $i - 3$ or $i - 4$ peptide carbonyl oxygen may induce or stabilize a 3–4° bend in a helix relative to Ala (49). This might cause significant changes in the TM segment that affect cation coordination. Interestingly, Thr^{132} of the *E. coli* Na^+/H^+ antiporter NhaA has been shown to participate in cation coordination (50), and other Ser or Thr residues have also been shown to be important in cation binding and transport in other membrane transporters (51–53). However, experiments on the mammalian NHE1 isoform of the Na^+/H^+ exchanger show that not all Ser and Thr residues are important in this regard (9, 15).

The ability of a Ser to substitute for Thr^{144} is not unprecedented. Amino acids 124–156 of the related *Zygosaccharomyces rouxii* Na^+/H^+ exchanger are strikingly similar to amino acids 125–158 of *S. pombe* Sod2. Amino acids Thr^{141} and

Thr^{143} of *Zr*Sod2-22p align with amino acids Thr^{142} and Thr^{144} of Sod2, respectively (Fig. 1*B*). Previous studies have demonstrated that T141S and S150T mutations of *Zr*Sod2-22p altered and broadened the cation selectivity of this antiporter and demonstrated that the presence of hydroxyl groups was critical for cation transport (54). Pro^{145}, which aligns with Sod2 Pro^{146}, was also shown to be important in substrate specificity. We found that the downstream Thr^{144} of Sod2 rather than Thr^{142} of Sod2 had a role similar to that of Thr^{141} of *Zr*Sod2-22p. These results suggest that Thr^{144} plays a functional role similar to that of Thr^{141} of *Zr*Sod2-22p despite the fact that it does not align precisely with amino acid Thr^{141} of *Zr*Sod2-22p.

In contrast to Thr^{144}, mutation of the amino acids Leu^{132}, Gly^{133}, Ser^{134}, Leu^{135}, Leu^{136}, and Gly^{139} (Group II; Table 1) exhibited phenotypes with slightly depressed growth in both NaCl- and LiCl-containing media. Although the effect is small, this region is conserved in both human NHE1 and *Zr*Sod2-22p (54) (Fig. 1). These residues are located in helical regions in the NMR structure, and it may be that changes in amino acid packing or helix structure lead to less efficient transport and therefore reduced resistance.

To help explain the functional results, we expressed and purified Sod2 TM IV and analyzed the structure of the protein using NMR. Earlier studies have demonstrated that the amino acid sequences of TM segments of membrane proteins contain most of the required structural information needed to form their native structures (55–58). This approach has been used successfully previously for mammalian NHE1 (15, 16) and for the membrane domain of CorA (59).

NMR experiments revealed significant secondary structure information. Hα chemical shifts and $^{3}J_{\mathrm{HNH}\alpha}$ coupling constants (supplemental Fig. 7) suggested that TM IV contains two helical regions separated by an extended segment. Although the N-terminal portion of the TM IV peptide showed largely helical character, Hα chemical shift deviations of residues 133 and 139 were closer to random coil values (Table 1), which could suggest that this N-terminal helix is broken, distorted, or dynamic at these positions. The low number of helical distances observed in the NOESY spectrum (supplemental Fig. 8) could be a further indication of dynamic behavior or distortion of the helices. This could simply be a result of the peptide being in organic solvent rather than in a membrane or perhaps indicates the importance of other transmembrane segments that might stabilize partially unwound helices in the tertiary structure.

Additionally, although data for Pro^{146} could not be observed, it is predicted to be a helix breaker (60). This is not unprecedented as the structure of hNHE1 TM IV shows two proline residues that disrupt the helix and form an extended section (20). Most interestingly, the functionally critical Sod2 residues Thr^{144}, Val^{147}, and Asp^{145} and residue Pro^{146} (shown earlier) are found in or very close to the extended region (Table 1). This is consistent with the results of other structural studies that have shown that discontinuous membrane helices are often involved in substrate coordination, for example *E. coli* NhaA (50, 61).

Although the data were not sufficient to calculate a precise structure, a model of Sod2 TM IV was created using Xplor-NIH (31) to better visualize the secondary structure and to provide a basis for comparison with other published structures. We suggest that TM IV of Sod2 may be structurally and functionally more similar to TM VI of NHE1 than to TM IV of NHE1 based on analysis of amino acid alignments, data examining critical amino acids in these helices, and the overall structure of the regions. Both contain two helices with an intervening unwound region that is critical in function (15). TM IV of human NHE1 has an unwound region, but this is flanked by only one helix (16).

Assessment of functional properties of aligned residues also supports the hypothesis that TM IV of Sod2 is similar to TM VI of NHE1. Mutation of residues Asp^{238} and Pro^{239} of human NHE1 results in a non-functional protein. These residues correspond to Asp^{145} and Pro^{146} in Sod2 that are also critical to function (4, 17). Similarly, the mutation of Val^{237} of NHE1 to Cys had reduced function in the presence of cysteine-modifying compounds, and this amino acid corresponds to Thr^{144} of Sod2 that is also critical to function.

We have also noted earlier that TM VI of NHE1 is similar to TM IV of NhaA (15). Comparison of Sod2 TM IV with *E. coli* NhaA TM IV also suggests that although they have different primary structures their secondary structures are similar, both having a helix-unwound region-helix configuration (Fig. 10*C*). Interestingly, TM IV of *E. coli* NhaA also contains important residues in this segment as mutation of either Thr^{132} or Asp^{133} has large effects on the apparent K_m, indicating a role in the integrity of the transport mechanism (6, 62). The extended peptide region may help accommodate the charged ion substrate (50).

To assess the effect these mutations might have on the folded structure and to provide evidence that the deduced structure of Sod2 TM IV is valid, we constructed a homology model of the membrane domain of Sod2. Mounting evidence suggests that a finite number of folds exist for membrane transporters (63) and that proteins with quite different primary amino acid sequences can have surprisingly similar structures. For example, the bile acid sodium symporter of *Neisseria meningitides* has a low primary sequence identity to *E. coli* NhaA, but the structure is surprisingly similar to that of NhaA (59).

With this justification, we decided to use the functionally related NhaA structure as a template for homology modeling of Sod2. After several iterative rounds of modeling, we obtained a model that satisfies our NMR data and the collected biochemical data (Fig. 10*A*). The model is largely free of steric conflicts as demonstrated by 98% of residues falling within the acceptable regions of the Ramachandran plot and the remaining residues falling in flexible regions of the structure (Fig. 10). Additionally, analysis using the ConSurf method (38, 39) indicates that functionally important regions on the interior of the transporter show the highest levels of conservation (supplemental Fig. 10) including the unwound section of TM IV. This method was also used to validate a model structure of NHE1 (40, 64).

The overall architecture of the model of Sod2 indicates the same fold as NhaA (6) with helices IV and XI having an unwound, crossed configuration in the membrane (Fig. 10*B*). Functionally critical residues His^{367}, Asp^{241}, (3), Pro^{146} (4), Asp^{145}, and Glu^{173} (18) are all situated in or near the putative transport pore (Fig. 10*E*). The exceptions are residues Asp^{266}

and Asp^{267}. These residues were found to be critically important for transport activity (3) but are not located near the transport site. They are located on a short α-helix within a long extracellular loop. A possible explanation is that this long loop may form a "caplike" structure on the cytoplasmic side of the pore opening. The negative charges could help attract sodium ions for transport. Because this is not a feature found in NhaA, it would be unlikely to be predicted by molecular modeling.

Significantly, the critical residues in the model of TM IV, Thr^{144}–Pro^{146}, are in an extended conformation and face the hypothetical transport pore in agreement with our deduced NMR structure. This offers further evidence that these residues are involved in ion translocation and supports the NMR structure we obtained (Fig. 10*C*). Val^{147}, however, is in a helical conformation and faces toward the outer helices in the homology model. From the homology model, one possible explanation of the functional defect of V147A is that mutation at this site affects helical packing, likely destabilizing the structure, leading to a functional defect. This is supported by our confocal data that suggest that V147A is targeted the same as the wild type protein and by our trypsinolysis data that show that V147A is more susceptible to digestion, suggesting increased flexibility. Alternatively, Val has a lower propensity to form helices than either Ala or Leu; therefore, these mutations may lead to increased helical character, perturbing the placement of TM IV in the membrane or decreasing the flexibility of the segment, preventing proper function (65). This is still consistent with the trypsin digestion data as the change in secondary structure could again alter helix packing and flexibility. In contrast, the NMR data and structure suggest that Val^{147} is extended or only weakly helical in conformation. This suggests that Val^{147} may be more conformationally dynamic than the Ala and Leu mutants and that this flexibility is required for proper function. The fact that Val^{147} is extended in the NMR structure and helical in the homology model (Table 1) further suggests that this position is likely locally flexible and requires the full membrane domain to form proper folded helical contacts.

In summary, the deduced secondary structure of the peptide based on NMR data consists of a slightly kinked N-terminal helix at residues 128–142 followed by a very flexible extended segment at residues 143–146 and a short C-terminal helix at residues 147–154. This secondary structure is supported by a homology model of TM IV of Sod2 derived from *E. coli* NhaA. The functional data suggest that residues 144–146 appear to have analogous partners in *E. coli* NhaA, human NHE1, and *Zr*Sod2-22p, indicating the importance of this region in transport. The salt tolerance protein Sod2 has a partially unwound helix containing functionally important residues for ion transport, consistent with results obtained with human NHE1 and *E. coli* NhaA. This study extends our current molecular understanding of salt tolerance and salt tolerance proteins. Previously we demonstrated that mutation of Asp^{145} (17) and Pro^{146} (4) of Sod2 resulted in a transport defect that was unable to confer salt tolerance. Our present results demonstrate that the flanking amino acids Thr^{144} and Val^{147} are also critical for Sod2 structure and function and that TM IV is likely to be directly involved in ion translocation. We have also demonstrated that the hydroxyl of Thr^{144} is required for activity and that the conservative Thr to Ser mutation results in the inability to transport Na^+ while maintaining Li^+ transport. We suggest that TM IV of Sod2 serves a role similar to that of TM IV of *E. coli* NhaA and TM VI of human NHE1.

Acknowledgment—We are grateful for the gift of an anti-H^+-ATPase antibody from Dr. C. Slayman, Yale School of Medicine.

REFERENCES

1. Jia, Z.-P., McCullough, N., Martel, R., Hemmingsen, S., and Young, P. G. (1992) Gene amplification at a locus encoding a putative Na^+/H^+ antiporter confers sodium and lithium tolerance in fission yeast. *EMBO J.* **11,** 1631–1640
2. Haworth, R. S., Lemire, B. D., Crandall, D., Cragoe, E. J., Jr., and Fliegel, L. (1991) Characterization of proton fluxes across the cytoplasmic membrane of the yeast *Saccharomyces cerevisiae*. *Biochim. Biophys. Acta* **1098,** 79–89
3. Dibrov, P., Young, P. G., and Fliegel, L. (1998) Functional analysis of amino acid residues essential for activity in the Na^+/H^+ exchanger of fission yeast. *Biochemistry* **37,** 8282–8288
4. Ndayizeye, M., Touret, N., and Fliegel, L. (2009) Proline 146 is critical to the structure, function and targeting of sod2, the Na^+/H^+ exchanger of *Schizosaccharomyces pombe*. *Biochim. Biophys. Acta* **1788,** 983–992
5. Brett, C. L., Donowitz, M., and Rao, R. (2005) Evolutionary origins of eukaryotic sodium/proton exchangers. *Am. J. Physiol. Cell Physiol.* **288,** C223–C239
6. Hunte, C., Screpanti, E., Venturi, M., Rimon, A., Padan, E., and Michel, H. (2005) Structure of a Na^+/H^+ antiporter and insights into mechanism of action and regulation by pH. *Nature* **435,** 1197–1202
7. Xiang, M., Feng, M., Muend, S., and Rao, R. (2007) A human Na^+/H^+ antiporter sharing evolutionary origins with bacterial NhaA may be a candidate gene for essential hypertension. *Proc. Natl. Acad. Sci. U.S.A.* **104,** 18677–18681
8. Schushan, M., Xiang, M., Bogomiakov, P., Padan, E., Rao, R., and Ben-Tal, N. (2010) Model-guided mutagenesis drives functional studies of human NHA2, implicated in hypertension. *J. Mol. Biol.* **396,** 1181–1196
9. Ding, J., Rainey, J. K., Xu, C., Sykes, B. D., and Fliegel, L. (2006) Structural and functional characterization of transmembrane segment VII of the Na^+/H^+ exchanger isoform 1. *J. Biol. Chem.* **281,** 29817–29829
10. Lee, B. L., Li, X., Liu, Y., Sykes, B. D., and Fliegel, L. (2009) Structural and functional analysis of transmembrane XI of the NHE1 isoform of the Na^+/H^+ exchanger. *J. Biol. Chem.* **284,** 11546–11556
11. Lee, B. L., Li, X., Liu, Y., Sykes, B. D., and Fliegel, L. (2009) Structural and functional analysis of extracellular loop 2 of the Na^+/H^+ exchanger. *Biochim. Biophys. Acta* **1788,** 2481–2488
12. Lee, B. L., Sykes, B. D., and Fliegel, L. (2011) Structural analysis of the Na^+/H^+ exchanger isoform 1 (NHE1) using the divide and conquer approach. *Biochem. Cell Biol.* **89,** 189–199
13. Reddy, T., Ding, J., Li, X., Sykes, B. D., Rainey, J. K., and Fliegel, L. (2008) Structural and functional characterization of transmembrane segment IX of the NHE1 isoform of the Na^+/H^+ exchanger. *J. Biol. Chem.* **283,** 22018–22030
14. Slepkov, E. R., Rainey, J. K., Sykes, B. D., and Fliegel, L. (2007) Structural and functional analysis of the Na^+/H^+ exchanger. *Biochem. J.* **401,** 623–633
15. Tzeng, J., Lee, B. L., Sykes, B. D., and Fliegel, L. (2010) Structural and functional analysis of transmembrane segment VI of the NHE1 isoform of the Na^+/H^+ exchanger. *J. Biol. Chem.* **285,** 36656–36665
16. Slepkov, E. R., Rainey, J. K., Li, X., Liu, Y., Cheng, F. J., Lindhout, D. A., Sykes, B. D., and Fliegel, L. (2005) Structural and functional characterization of transmembrane segment IV of the NHE1 isoform of the Na^+/H^+ exchanger. *J. Biol. Chem.* **280,** 17863–17872
17. Wiebe, C. A., Rieder, C., Young, P. G., Dibrov, P., and Fliegel, L. (2003)

Functional analysis of amino acids of the Na^+/H^+ exchanger that are important for proton translocation. *Mol. Cell. Biochem.* **254,** 117–124
18. Fliegel, L. (2005) Identification of conserved polar residues important for salt tolerance by the Na^+/H^+ exchanger of *Schizosaccharomyces pombe*. *Mol. Cell. Biochem.* **268,** 83–92
19. Fliegel, L., Wiebe, C., Chua, G., and Young, P. G. (2005) Functional expression and cellular localization of the Na^+/H^+ exchanger Sod2 of the fission yeast *Schizosaccharomyces pombe*. *Can J. Physiol. Pharmacol.* **83,** 565–572
20. Slepkov, E. R., Chow, S., Lemieux, M. J., and Fliegel, L. (2004) Proline residues in transmembrane segment IV are critical for activity, expression and targeting of the Na^+/H^+ exchanger isoform 1. *Biochem. J.* **379,** 31–38
21. Silva, N. L., Wang, H., Harris, C. V., Singh, D., and Fliegel, L. (1997) Characterization of the Na^+/H^+ exchanger in human choriocarcinoma (BeWo) cells. *Pflugers Arch.* **433,** 792–802
22. Rieder, C. V., and Fliegel, L. (2002) Developmental regulation of Na^+/H^+ exchanger expression in fetal and neonatal mice. *Am. J. Physiol. Heart Circ. Physiol.* **283,** H273–H283
23. Dibrov, P., Smith, J. J., Young, P. G., and Fliegel, L. (1997) Identification and localization of the sod2 gene product in fission yeast. *FEBS Lett.* **405,** 119–124
24. Douglas, J. L., Trieber, C. A., Afara, M., and Young, H. S. (2005) Rapid, high-yield expression and purification of Ca^{2+}-ATPase regulatory proteins for high-resolution structural studies. *Protein Expr. Purif.* **40,** 118–125
25. Kay, L. E., Keifer, P., and Saarinen, T. (1992) Pure absorption gradient enhanced heteronuclear single quantum correlation spectroscopy with improved sensitivity. *J. Am. Chem. Soc.* **114,** 10663–10665
26. Zhang, O., Kay, L. E., Olivier, J. P., and Forman-Kay, J. D. (1994) Backbone ^1H and ^{15}N resonance assignments of the N-terminal SH3 domain of drk in folded and unfolded states using enhanced-sensitivity pulsed field gradient NMR techniques. *J. Biomol. NMR* **4,** 845–858
27. Vuister, G. W., and Bax, A. (1993) Quantitative *J* correlation: a new approach for measuring homonuclear 3-bond $J(H^NH^\alpha)$ coupling-constants in N-15-enriched proteins. *J. Am. Chem. Soc.* **115,** 7772–7777
28. Grzesiek, S., Kuboniwa, H., Hinck, A. P., and Bax, A. (1995) Multiple-quantum line narrowing for measurement of H^α-H^β *J* couplings in isotopically enriched proteins. *J. Am. Chem. Soc.* **117,** 5312–5315
29. Delaglio, F., Grzesiek, S., Vuister, G. W., Zhu, G., Pfeifer, J., and Bax, A. (1995) NMRPipe: a multidimensional spectral processing system based on UNIX pipes. *J. Biomol. NMR* **6,** 277–293
30. Johnson, B. A., and Blevins, R. A. (1994) NMRView: a computer program for the visualization and analysis of NMR data. *J. Biomol. NMR* **4,** 603–614
31. Schwieters, C. D., Kuszewski, J. J., Tjandra, N., and Clore, G. M. (2003) The Xplor-NIH NMR molecular structure determination package. *J. Magn. Reson.* **160,** 65–73
32. Eswar, N., Webb, B., Marti-Renom, M. A., Madhusudhan, M. S., Eramian, D., Shen, M. Y., Pieper, U., and Sali, A. (2006) Comparative protein structure modeling using Modeller. *Curr. Protoc. Bioinformatics* **Chapter 5,** Unit 5.6
33. Sievers, F., Wilm, A., Dineen, D., Gibson, T. J., Karplus, K., Li, W., Lopez, R., McWilliam, H., Remmert, M., Söding, J., Thompson, J. D., and Higgins, D. G. (2011) Fast, scalable generation of high-quality protein multiple sequence alignments using Clustal Omega. *Mol. Syst. Biol.* **7,** 539
34. Goujon, M., McWilliam, H., Li, W., Valentin, F., Squizzato, S., Paern, J., and Lopez, R. (2010) A new bioinformatics analysis tools framework at EMBL-EBI. *Nucleic Acids Res.* **38,** W695–W699
35. Krogh, A., Larsson, B., von Heijne, G., and Sonnhammer, E. L. (2001) Predicting transmembrane protein topology with a hidden Markov model: application to complete genomes. *J. Mol. Biol.* **305,** 567–580
36. Cole, C., Barber, J. D., and Barton, G. J. (2008) The Jpred 3 secondary structure prediction server. *Nucleic Acids Res.* **36,** W197–W201
37. Bhattacharya, A., Tejero, R., and Montelione, G. T. (2007) Evaluating protein structures determined by structural genomics consortia. *Proteins* **66,** 778–795
38. Landau, M., Mayrose, I., Rosenberg, Y., Glaser, F., Martz, E., Pupko, T., and Ben-Tal, N. (2005) ConSurf 2005: the projection of evolutionary conservation scores of residues on protein structures. *Nucleic Acids Res.* **33,** W299–W302
39. Glaser, F., Pupko, T., Paz, I., Bell, R. E., Bechor-Shental, D., Martz, E., and Ben-Tal, N. (2003) ConSurf: identification of functional regions in proteins by surface-mapping of phylogenetic information. *Bioinformatics* **19,** 163–164
40. Ashkenazy, H., Erez, E., Martz, E., Pupko, T., and Ben-Tal, N. (2010) ConSurf 2010: calculating evolutionary conservation in sequence and structure of proteins and nucleic acids. *Nucleic Acids Res.* **38,** W529–W533
41. Wiebe, C. A., Dibattista, E. R., and Fliegel, L. (2001) Functional role of amino acid residues in Na^+/H^+ exchangers. *Biochem. J.* **357,** 1–10
42. Shi, H., Ishitani, M., Kim, C., and Zhu, J. K. (2000) The *Arabidopsis thaliana* salt tolerance gene SOS1 encodes a putative Na^+/H^+ antiporter. *Proc. Natl. Acad. Sci. U.S.A.* **97,** 6896–6901
43. Murtazina, R., Booth, B. J., Bullis, B. L., Singh, D. N., and Fliegel, L. (2001) Functional analysis of polar amino-acid residues in membrane associated regions of the NHE1 isoform of the mammalian Na^+/H^+ exchanger. *Eur. J. Biochem.* **268,** 4674–4685
44. Dibrov, P., and Fliegel, L. (1998) Comparative molecular analysis of Na^+/H^+ exchangers: a unified model for Na^+/H^+ antiport? *FEBS Lett.* **424,** 1–5
45. Wishart, D. S., Bigam, C. G., Holm, A., Hodges, R. S., and Sykes, B. D. (1995) ^1H, ^{13}C and ^{15}N random coil NMR chemical shifts of the common amino acids. I. Investigations of nearest-neighbor effects. *J. Biomol. NMR* **5,** 67–81
46. Kemp, G., Young, H., and Fliegel, L. (2008) Structure and function of the human Na^+/H^+ exchanger isoform 1. *Channels* **2,** 329–336
47. Padan, E. (2008) The enlightening encounter between structure and function in the NhaA Na^+-H^+ antiporter. *Trends Biochem. Sci.* **33,** 435–443
48. Fleming, K. G., and Engelman, D. M. (2001) Specificity in transmembrane helix-helix interactions can define a hierarchy of stability for sequence variants. *Proc. Natl. Acad. Sci. U.S.A.* **98,** 14340–14344
49. Ballesteros, J. A., Deupi, X., Olivella, M., Haaksma, E. E., and Pardo, L. (2000) Serine and threonine residues bend α-helices in the $\chi_1 = g^-$ conformation. *Biophys. J.* **79,** 2754–2760
50. Padan, E., Kozachkov, L., Herz, K., and Rimon, A. (2009) NhaA crystal structure: functional-structural insights. *J. Exp. Biol.* **212,** 1593–1603
51. Díez-Sampedro, A., Wright, E. M., and Hirayama, B. A. (2001) Residue 457 controls sugar binding and transport in the Na^+/glucose cotransporter. *J. Biol. Chem.* **276,** 49188–49194
52. Kamiya, T., and Maeshima, M. (2004) Residues in internal repeats of the rice cation/H^+ exchanger are involved in the transport and selection of cations. *J. Biol. Chem.* **279,** 812–819
53. Li, H., and Pajor, A. M. (2003) Serines 260 and 288 are involved in sulfate transport by hNaSi-1. *J. Biol. Chem.* **278,** 37204–37212
54. Kinclova-Zimmermannova, O., Zavrel, M., and Sychrova, H. (2006) Importance of the seryl and threonyl residues of the fifth transmembrane domain to the substrate specificity of yeast plasma membrane Na^+/H^+ antiporters. *Mol. Membr. Biol.* **23,** 349–361
55. Cunningham, F., and Deber, C. M. (2007) Optimizing synthesis and expression of transmembrane peptides and proteins. *Methods* **41,** 370–380
56. Hunt, J. F., Earnest, T. N., Bousché, O., Kalghatgi, K., Reilly, K., Horváth, C., Rothschild, K. J., and Engelman, D. M. (1997) A biophysical study of integral membrane protein folding. *Biochemistry* **36,** 15156–15176
57. Katragadda, M., Alderfer, J. L., and Yeagle, P. L. (2001) Assembly of a polytopic membrane protein structure from the solution structures of overlapping peptide fragments of bacteriorhodopsin. *Biophys. J.* **81,** 1029–1036
58. Katragadda, M., Chopra, A., Bennett, M., Alderfer, J. L., Yeagle, P. L., and Albert, A. D. (2001) Structures of the transmembrane helices of the G-protein coupled receptor, rhodopsin. *J. Pept. Res.* **58,** 79–89
59. Hu, N. J., Iwata, S., Cameron, A. D., and Drew, D. (2011) Crystal structure of a bacterial homologue of the bile acid sodium symporter ASBT. *Nature* **478,** 408–411
60. Cordes, F. S., Bright, J. N., and Sansom, M. S. (2002) Proline-induced distortions of transmembrane helices. *J. Mol. Biol.* **323,** 951–960

61. Screpanti, E., and Hunte, C. (2007) Discontinuous membrane helices in transport proteins and their correlation with function. *J. Struct. Biol.* **159,** 261–267
62. Galili, L., Rothman, A., Kozachkov, L., Rimon, A., and Padan, E. (2002) Trans membrane domain IV is involved in ion transport activity and pH regulation of the NhaA-Na^+/H^+ antiporter of *Escherichia coli*. *Biochemistry* **41,** 609–617
63. Oberai, A., Ihm, Y., Kim, S., and Bowie, J. U. (2006) A limited universe of membrane protein families and folds. *Protein Sci.* **15,** 1723–1734
64. Landau, M., Herz, K., Padan, E., and Ben-Tal, N. (2007) Model structure of the Na^+/H^+ exchanger 1 (NHE1): functional and clinical implications. *J. Biol. Chem.* **282,** 37854–37863
65. Pace, C. N., and Scholtz, J. M. (1998) A helix propensity scale based on experimental studies of peptides and proteins. *Biophys. J.* **75,** 422–427

Table I (Supplement) Oligonucleotides used for site-directed mutagenesis of sod2. Mutated nucleotides are indicated in lowercase letters. Mutations resulting in changed amino acids have codons indicated in boldface type. Restriction sites that were introduced are underlined, and where indicated a site was removed (-). The forward oligonucleotide of the pair used for mutagenesis is shown.

Mutation	Oligos	Site
F126A	GCATATGCATTG**gcg**CCACAAATTAACTTTTTAG	*NarI*
P127A	GCATATGCATTGTTT**gCg**CAAATTAACTTTTTAG	*FspI*
Q128A	GCATATGCATTGTTcCCA**gcA**ATTAACTTTTTAGG	*BseYII*
I129A	CATATGCATTGTTTCCtCAg**gcT**AACTTTTTAGGATC	*Bsu36I*
N130A	GTTTCCACAAATT**gcC**TTTTTAGGATCcTTGCTGATCGCAGG	*BamHI*
F131A	CCACAAATTAAC**gcg**TTAGGATCTTTGC	*MluI*
L132A	CCACAAATTAACTTT**gcc**GGcTCTTTGCTGATCGC	*NaeI*
G133A	CAAATTAACTTTTTA**Gct**agcTTGCTGATCGCAGG	*NheI*
S134A	CAAATTAACTTTTTAGGA**gCT**cTGCTGATCGCAGG	*SacI*
L135A	CTTTTTAGGATCa**gcG**CTGATCGCAGGATG	*AfeI*
L136A	CTTTTTAGGATCTTTG**gcG**ATCGCAGGATGTATAAC	*PvuI*
I137A	GGATCTTTGCTG**gct**GCAGGATGTATAAC	*PstI*
G139A	CTTTGCTGATCGCA**GcA**TGcATAACTTCTACTGATC	*SphI*
C140A	GCTGATCGCAGGc**gcc**ATAACTTCTACTGATC	*NarI*
I141A	GCTGATCGCAGGATGc**gcA**ACTTCTACTGATCC	*FspI*
T142A	CGCAGGATGTATA**gCg**TCgACTGATCCTGTTC	*SalI*
S143A	GCAGGATGTATAACa**gCT**ACTGATCCTGTTC	*AlwNI*
T144A	GGATGTATAACTTCT**gCa**GATCCTGTTCTATC	*PstI*
T144D	*GGATGTATAACTTCT**gac**GATCCTGTcCTATCAGCATTG*	*Drd1*
T144K	*GGATGTATAACTTCT**Aag**GATCCTGTTCTATC*	*BamH1*
T144S	*GGATGTATAACTTCT**tCa**GATCCTGTTCTATC3*	*AlwN1*
V147A	GTATAACTTCTACgGATCCT**GcT**CTATCAGCATTGATTG	*BamHI*
V147L	GTATAACTTCTACgGATC**CTc**TTCTATCAGCATTG	*BamHI*
L148A	CTTCTACTGATCCTGTT**gct**agcGCATTGATTGTAGG	*NheI*
S149A	CTTCTACTGATCCTGTgCTA**gCA**GCATTGATTGTAG	*NheI*
L151A	CCTGTTCTATCAGCA**gcg**ATcGTAGGAGAAGGAGG	*PvuI*
L151S	CCTGTTCTATCAGCA**Tcg**ATcGTAGGAGAAGGAGG	*PvuI*
I152A	CCTGTTCTATCAGCgcTG**gcg**GTAGGAGAAGGAGGTC	*AfeI*

A

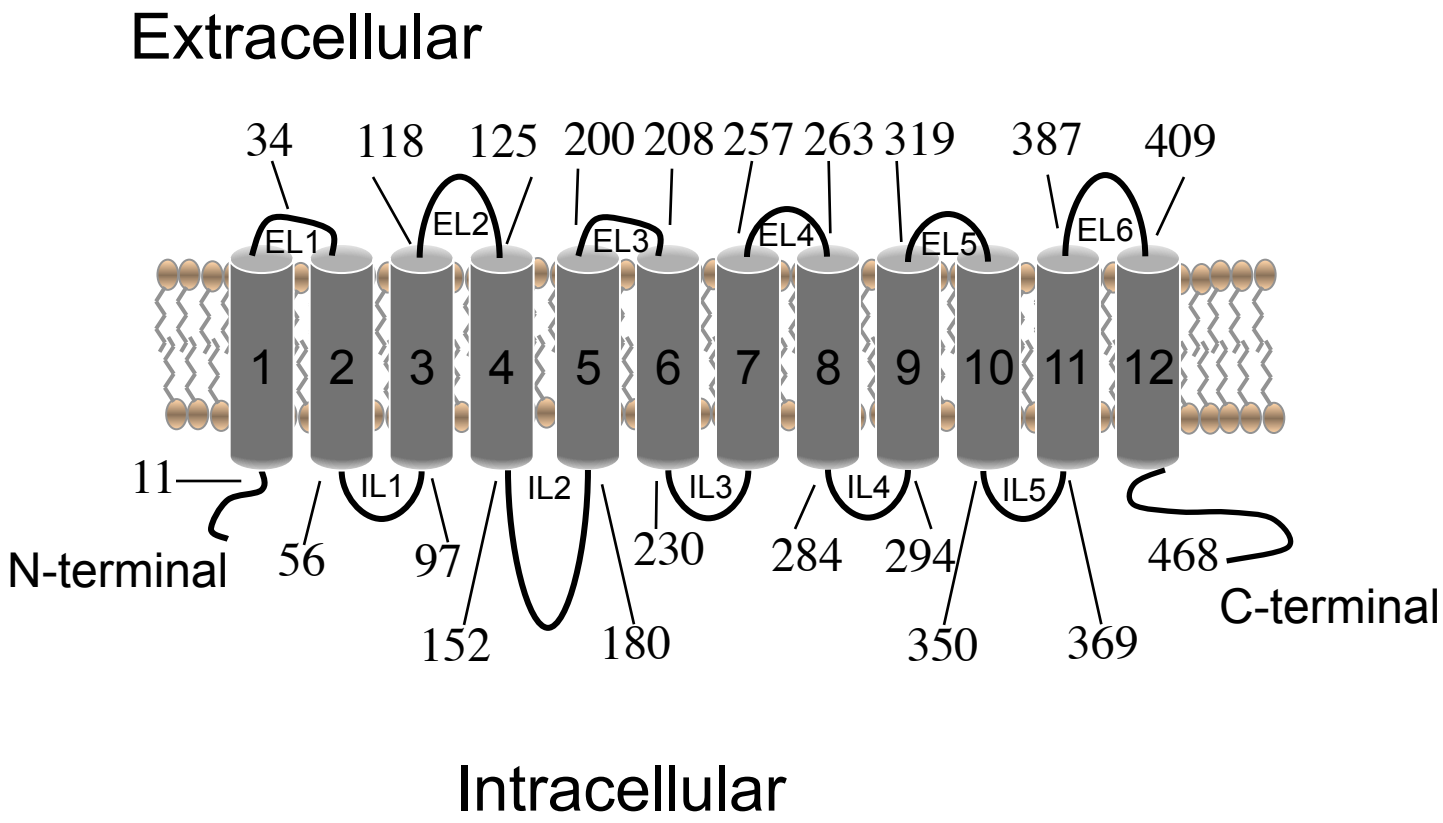

Fig. 1 Supplementary. Model of sod2. **A**. Topological model of sod2 based on hydrophobicity analysis (41). EL, extracellular loop; IL, intracellular loop.

B

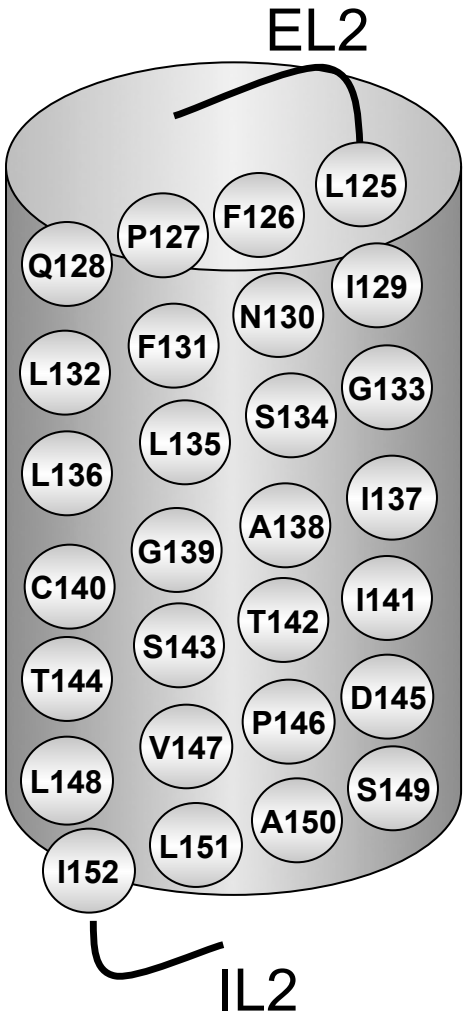

^{125}LFPQINFLGSLLIAGCITSTDPVLSALI^{152}

Fig. 1B Supplementary. **B**. Schematic diagram of amino acids present in TM IV of sod2.

Fig. 2 **A-D** supplementary. Growth of *S. pombe* containing either wild type or TM IV mutant sod2 proteins in liquid media with various concentrations of LiCl. All mutants, sod2 knock out (*Sod2::ura4)*, wild type sod2, growth in LiCl are shown. LiCl tolerance of strains was assessed by inoculating 2 X 10^6 cells into 2.5 ml of medium at 30 ^oC for up to 72 hours. Growth was assessed by measuring the absorbance of the cell suspensions at 600 nm at the indicated times. Results are the mean +/- SE of at least three determinations. *S. pombe* were grown in the presence of 0, 2, 5 or 10 mM LiCl. S2:U4 refers to *Sod2::ura4* (*S. pombe* with the sod2 knockout). Sod2 refers to *sod2::ura4* containing the wild type sod2 protein. In other cases the indicated sod2 TM IV mutant was introduced into S2:U4 and grown in the presence of 0, 2, 5 or 10 mM LiCl as indicated. **E**, Growth of *S. pombe* assessed as in A-D. All mutants were grown simultaneously in the same preparation of media. WTGFP, refers to the GFP fused sod2, equivalent to Sod2 measured in 2A. Sod2::Ura4 is *S. pombe* with the sod2 knockout. WTnoGFP, refers to the sod2 protein without the GFP tag, expressed as described earlier (3).

A

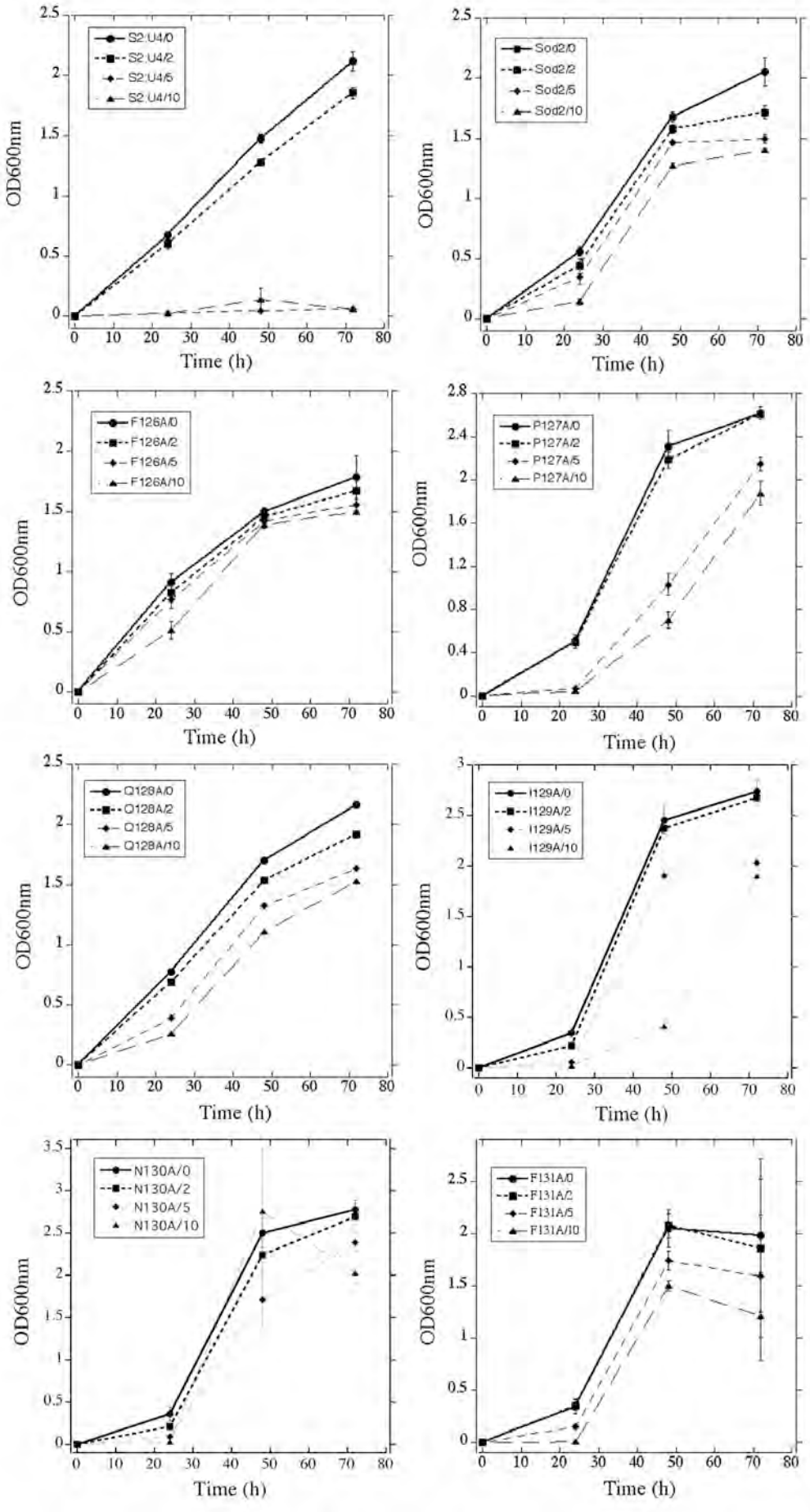
S2:U4/0
S2:U4/2
S2:U4/5
S2:U4/10
Sod2/0
Sod2/2
Sod2/5
Sod2/10
F126A/0
F126A/2
F126A/5
F126A/10
P127A/0
P127A/2
P127A/5
P127A/10
Q128A/0
Q128A/2
Q128A/5
Q128A/10
I129A/0
I129A/2
I129A/5
I129A/10
N130A/0
N130A/2
N130A/5
N130A/10
F131A/0
F131A/2
F131A/5
F131A/10
OD600nm
Time (h)

B

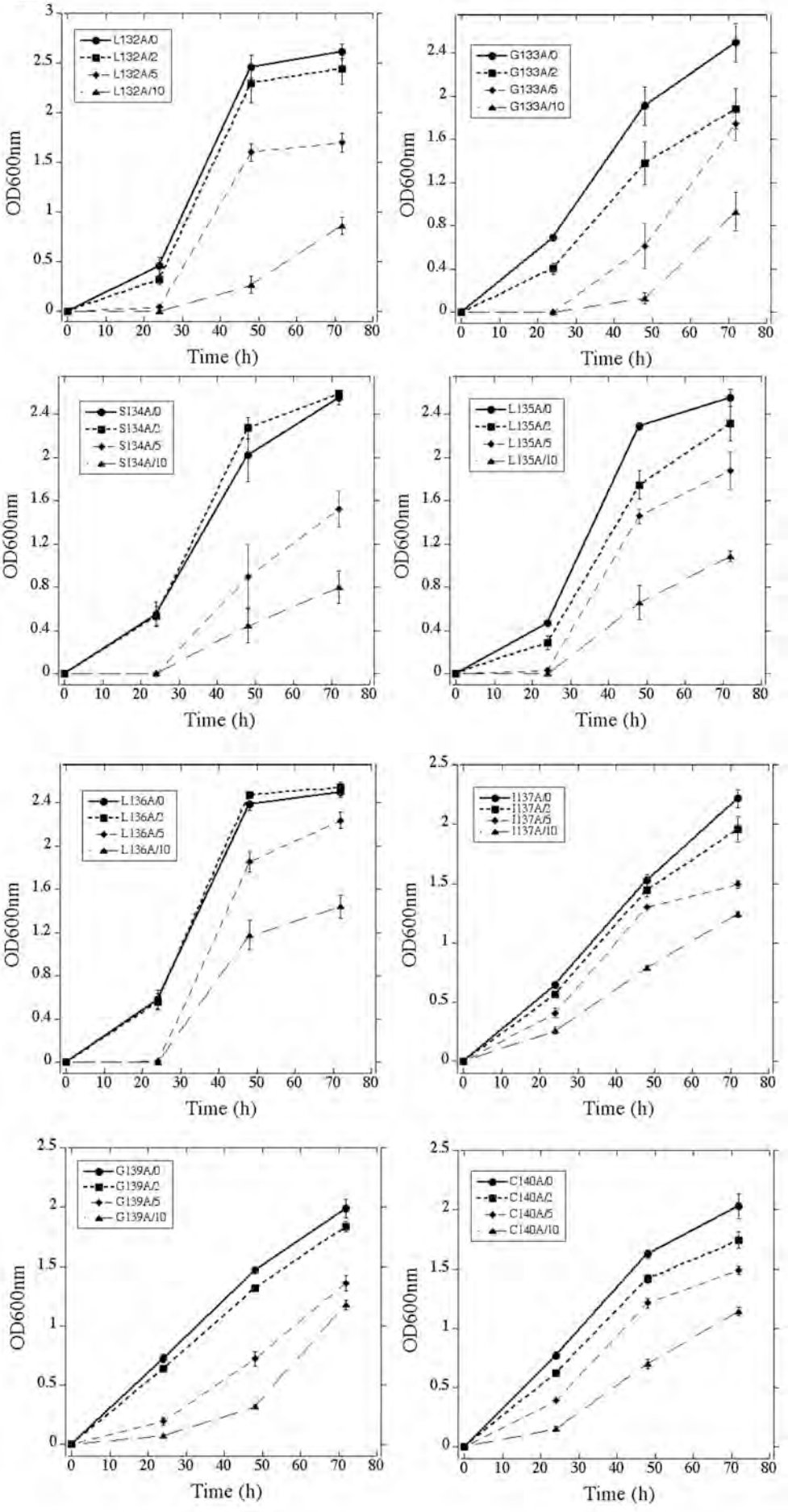
L132A/0
L132A/2
L132A/5
L132A/10
G133A/0
G133A/2
G133A/5
G133A/10
S134A/0
S134A/2
S134A/5
S134A/10
L135A/0
L135A/2
L135A/5
L135A/10
L136A/0
L136A/2
L136A/5
L136A/10
I137A/0
I137A/2
I137A/5
I137A/10
G139A/0
G139A/2
G139A/5
G139A/10
C140A/0
C140A/2
C140A/5
C140A/10
OD600nm
Time (h)

C

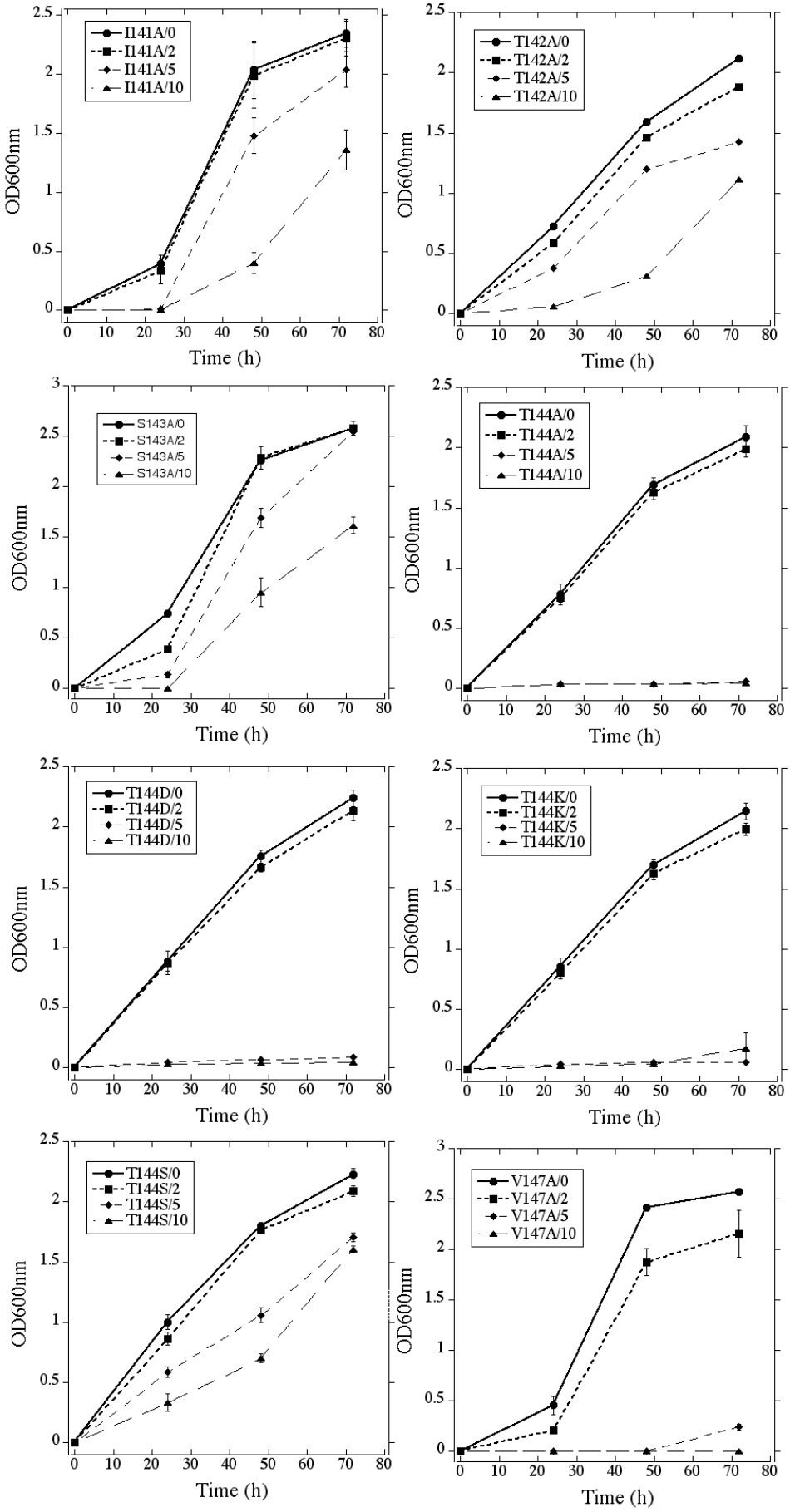
I141A/0
I141A/2
I141A/5
I141A/10
T142A/0
T142A/2
T142A/5
T142A/10
S143A/0
S143A/2
S143A/5
S143A/10
T144A/0
T144A/2
T144A/5
T144A/10
T144D/0
T144D/2
T144D/5
T144D/10
T144K/0
T144K/2
T144K/5
T144K/10
T144S/0
T144S/2
T144S/5
T144S/10
V147A/0
V147A/2
V147A/5
V147A/10
OD600nm
Time (h)

D

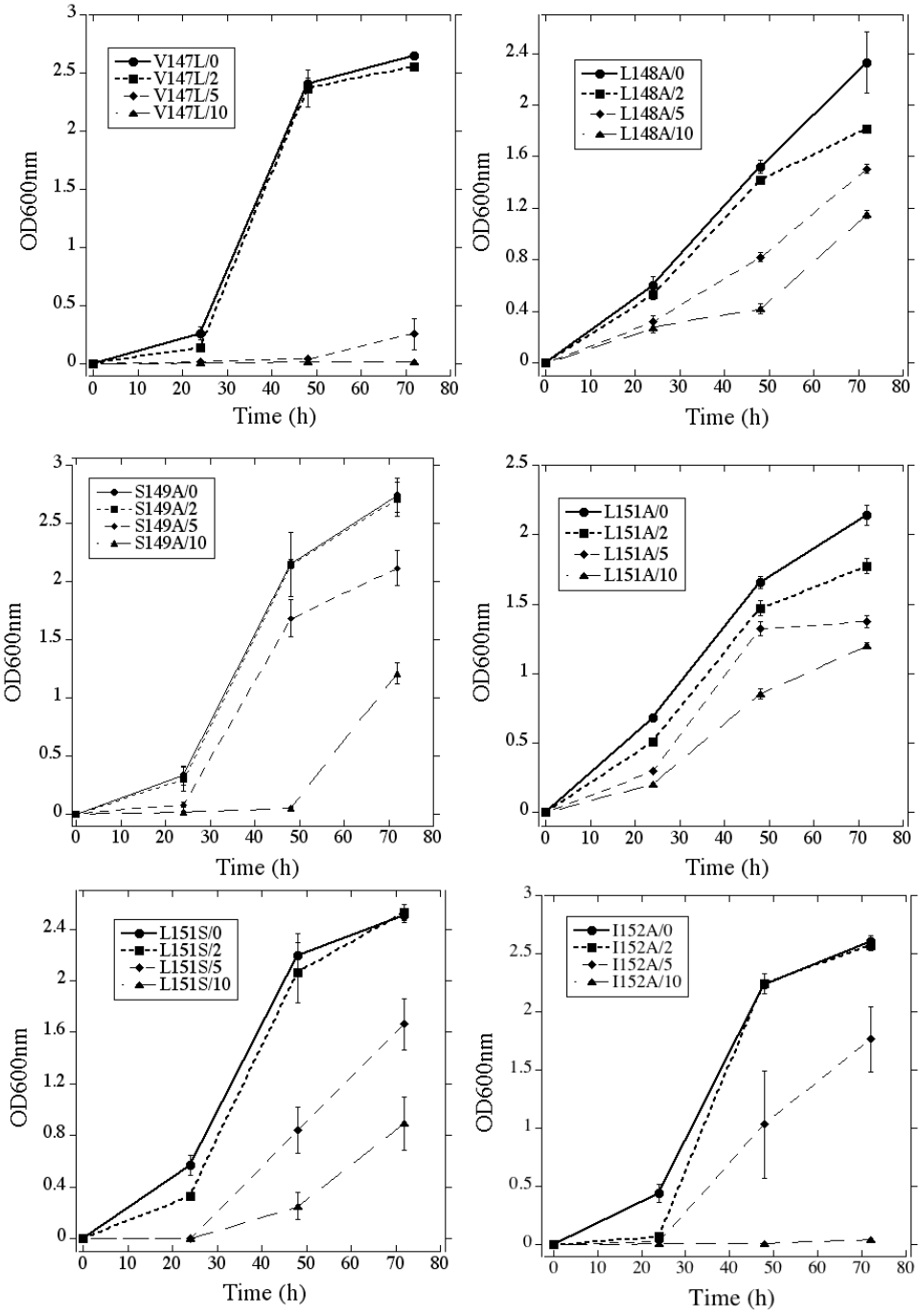
V147L/0
V147L/2
V147L/5
V147L/10
L148A/0
L148A/2
L148A/5
L148A/10
S149A/0
S149A/2
S149A/5
S149A/10
L151A/0
L151A/2
L151A/5
L151A/10
L151S/0
L151S/2
L151S/5
L151S/10
I152A/0
I152A/2
I152A/5
I152A/10
OD600nm
Time (h)

E

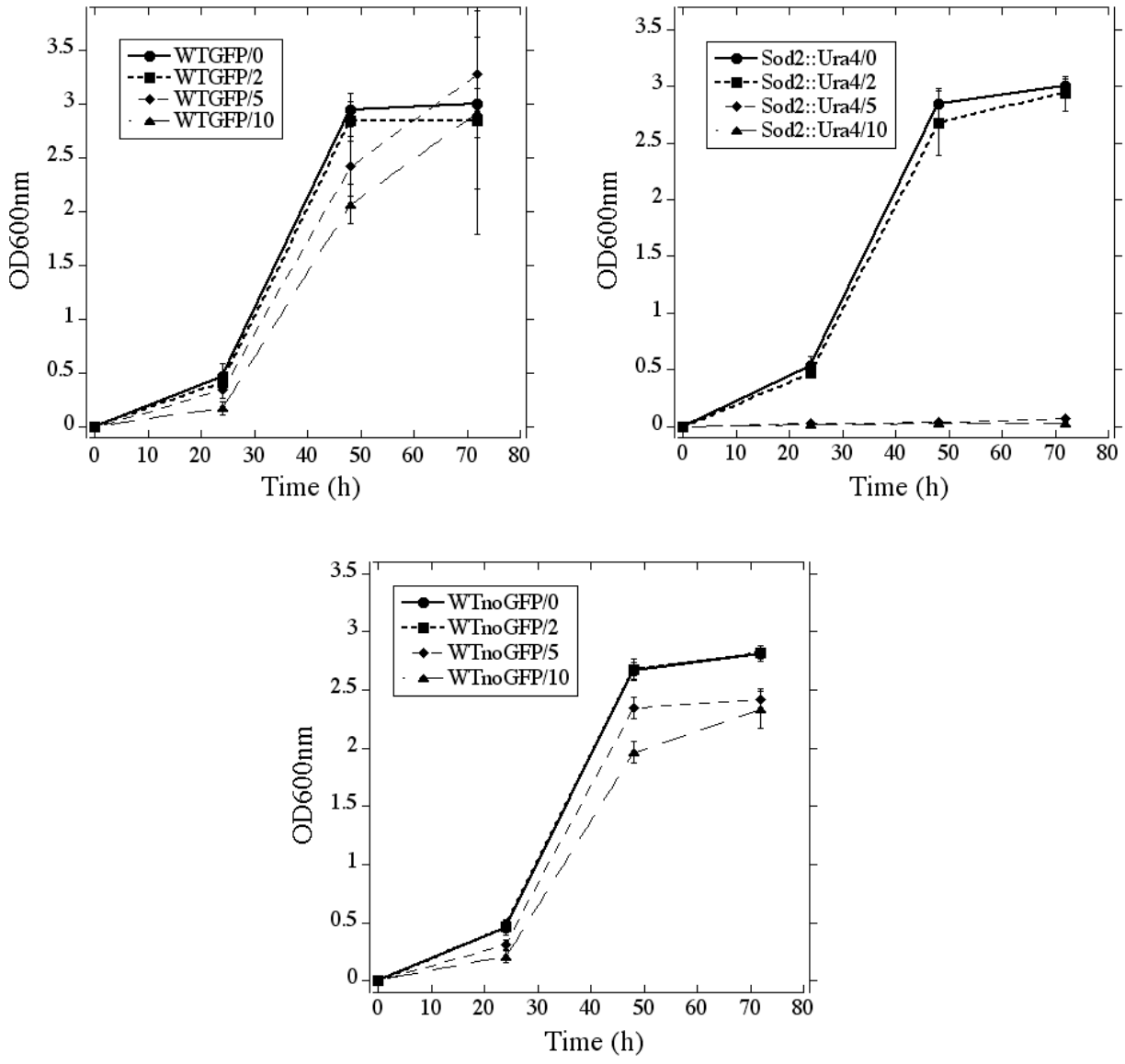
WTGFP/0
WTGFP/2
WTGFP/5
WTGFP/10
OD600nm
Time (h)
Sod2::Ura4/0
Sod2::Ura4/2
Sod2::Ura4/5
Sod2::Ura4/10
OD600nm
Time (h)
WTnoGFP/0
WTnoGFP/2
WTnoGFP/5
WTnoGFP/10
OD600nm
Time (h)

Fig. 3**A-D** supplementary. Growth of *S. pombe* containing either wild type or TM IV mutant sod2 proteins in liquid media with various concentrations of NaCl as described for supplementary Fig. 2. All mutants, sod2 knock out, (*Sod2::ura4, S2:U4)*, wild type sod2, growth in NaCl are shown. NaCl was added at concentrations of 0, 0.2 or 0.5 M as indicated. Results are the mean +/- SE of at least three determinations. **E**, Growth of *S. pombe* assessed as in A-D. All mutants were grown simultaneously in the same preparation of media. WTGFP, refers to the GFP fused sod2, equivalent to Sod2 measured in 3A. Sod2::Ura4 is *S. pombe* with the sod2 knockout. WTnoGFP, refers to the sod2 protein without the GFP tag, expressed as described earlier (3).

A

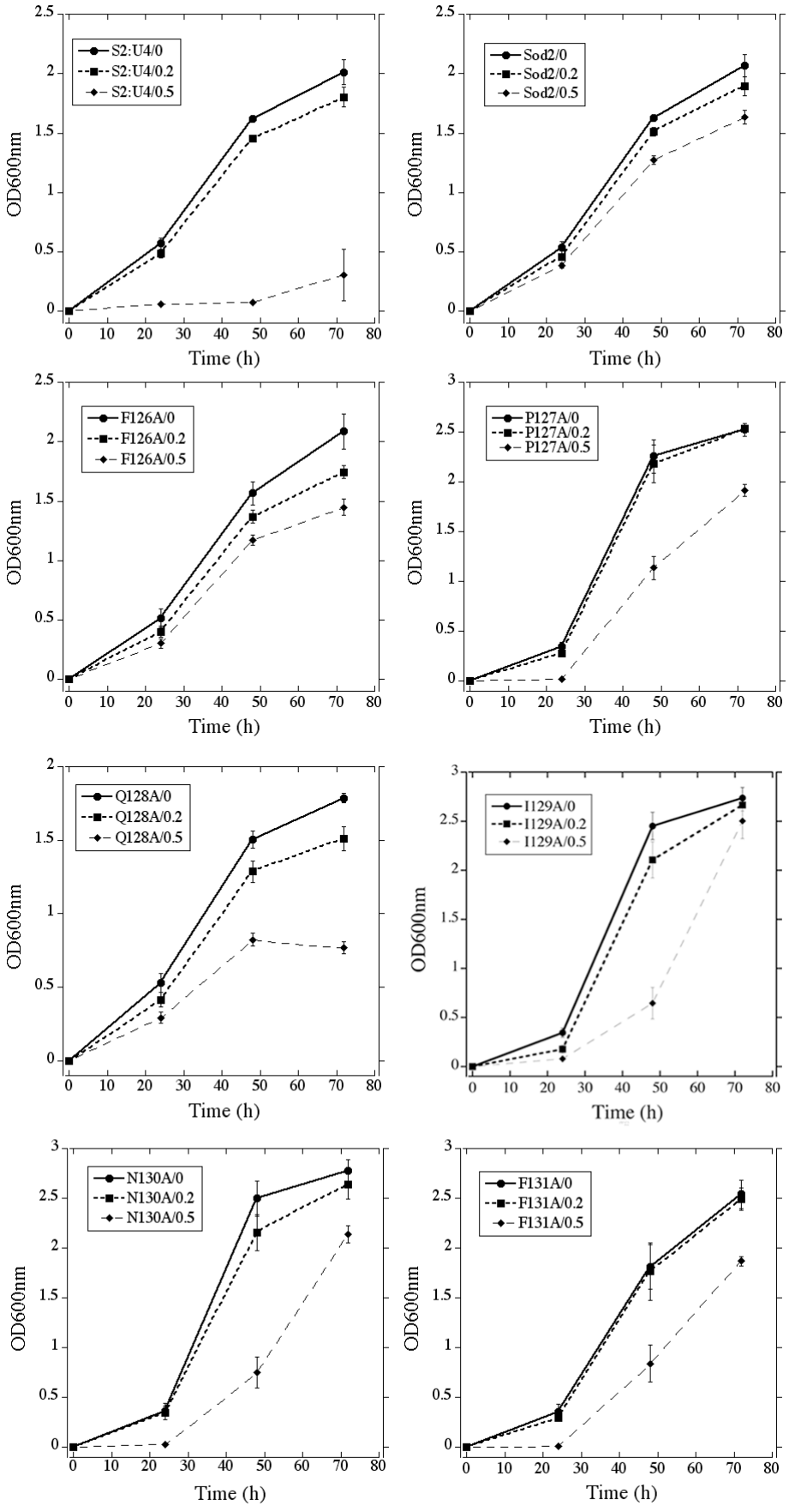
S2:U4/0
S2:U4/0.2
S2:U4/0.5
Sod2/0
Sod2/0.2
Sod2/0.5
F126A/0
F126A/0.2
F126A/0.5
P127A/0
P127A/0.2
P127A/0.5
Q128A/0
Q128A/0.2
Q128A/0.5
I129A/0
I129A/0.2
I129A/0.5
N130A/0
N130A/0.2
N130A/0.5
F131A/0
F131A/0.2
F131A/0.5
OD600nm
Time (h)

B

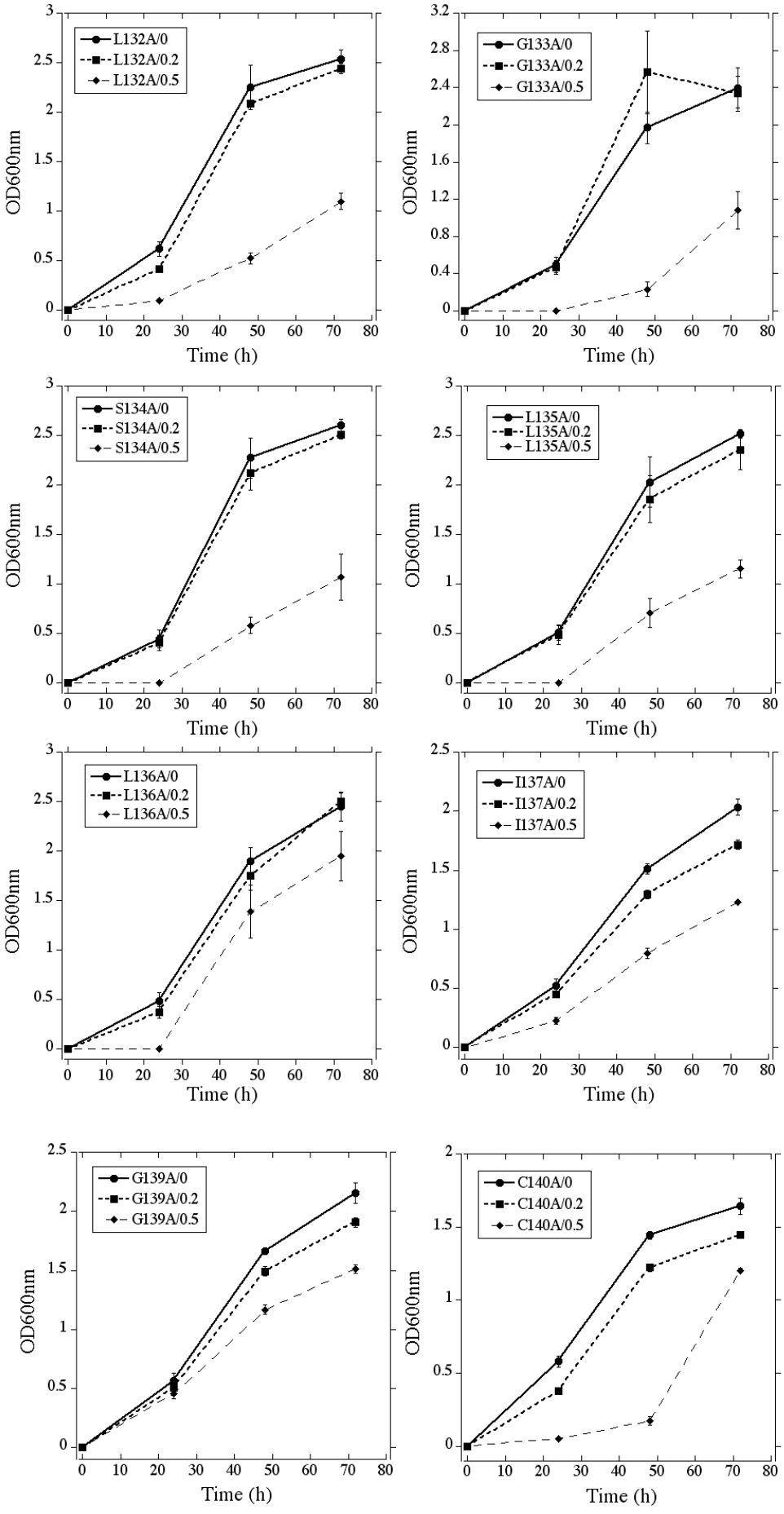
L132A/0
L132A/0.2
L132A/0.5
G133A/0
G133A/0.2
G133A/0.5
S134A/0
S134A/0.2
S134A/0.5
L135A/0
L135A/0.2
L135A/0.5
L136A/0
L136A/0.2
L136A/0.5
I137A/0
I137A/0.2
I137A/0.5
G139A/0
G139A/0.2
G139A/0.5
C140A/0
C140A/0.2
C140A/0.5
OD600nm
Time (h)

C

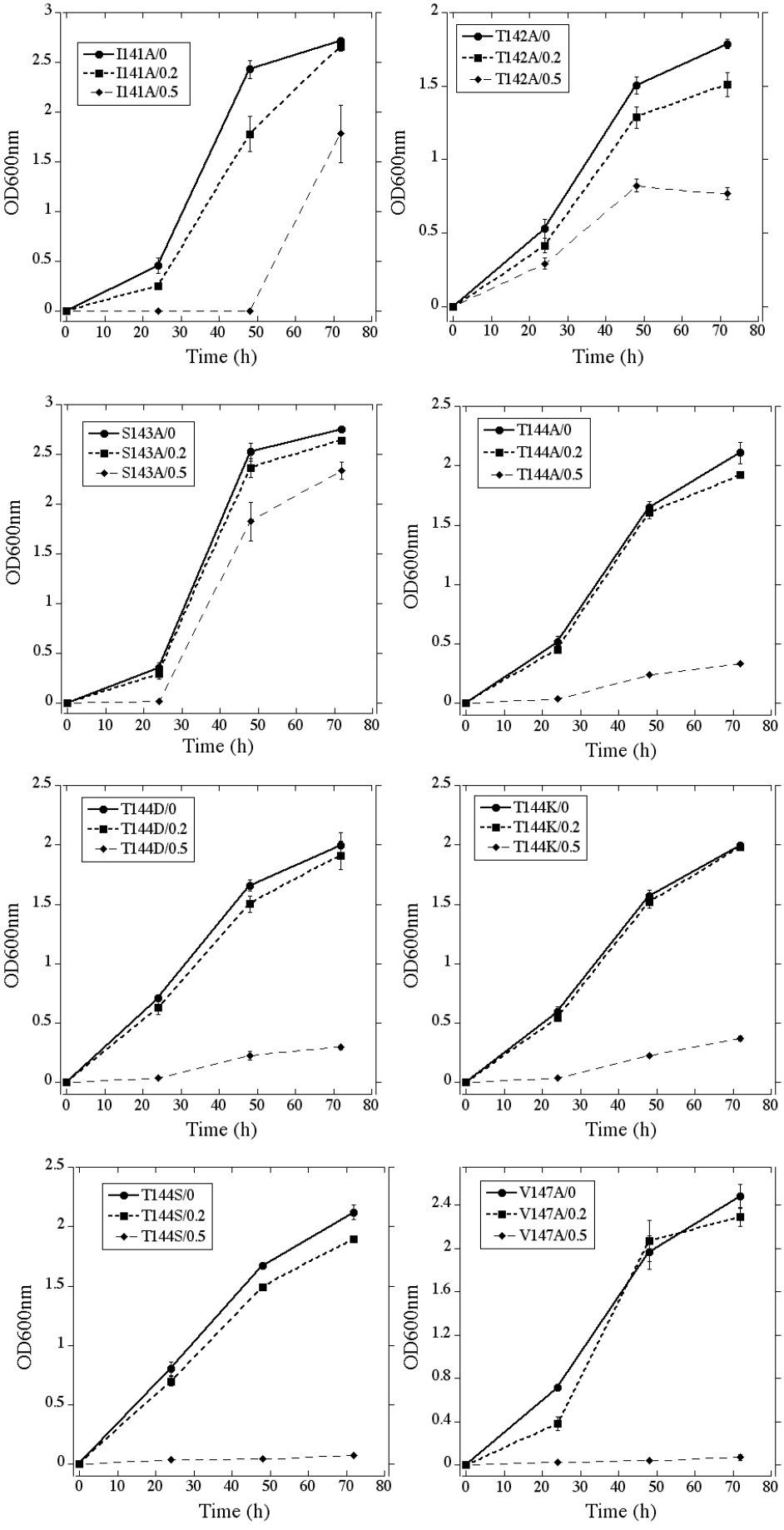
I141A/0
I141A/0.2
I141A/0.5
T142A/0
T142A/0.2
T142A/0.5
S143A/0
S143A/0.2
S143A/0.5
T144A/0
T144A/0.2
T144A/0.5
T144D/0
T144D/0.2
T144D/0.5
T144K/0
T144K/0.2
T144K/0.5
T144S/0
T144S/0.2
T144S/0.5
V147A/0
V147A/0.2
V147A/0.5
OD600nm
Time (h)

D

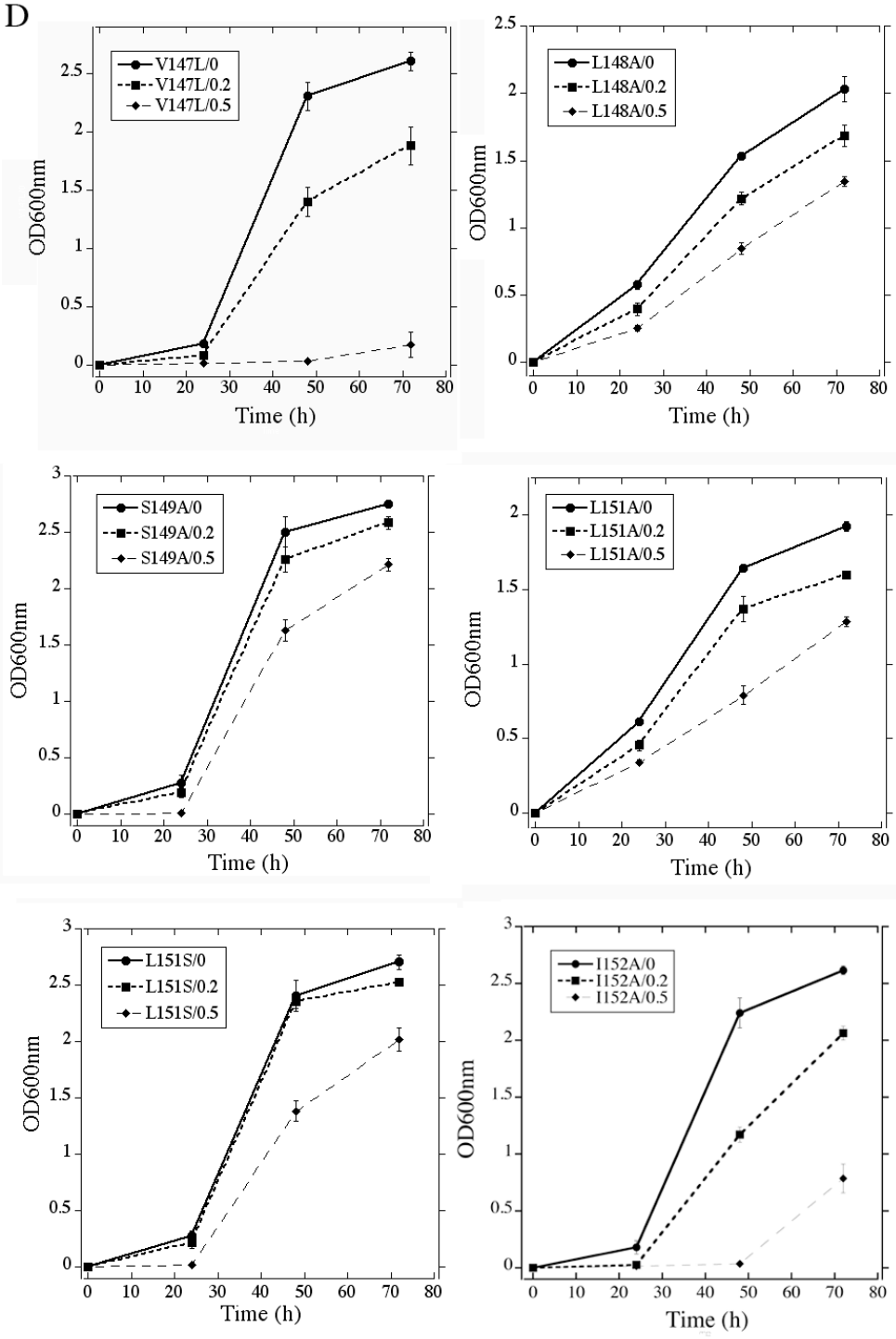
V147L/0
V147L/0.2
V147L/0.5
L148A/0
L148A/0.2
L148A/0.5
S149A/0
S149A/0.2
S149A/0.5
L151A/0
L151A/0.2
L151A/0.5
L151S/0
L151S/0.2
L151S/0.5
I152A/0
I152A/0.2
I152A/0.5
OD600nm
Time (h)

E

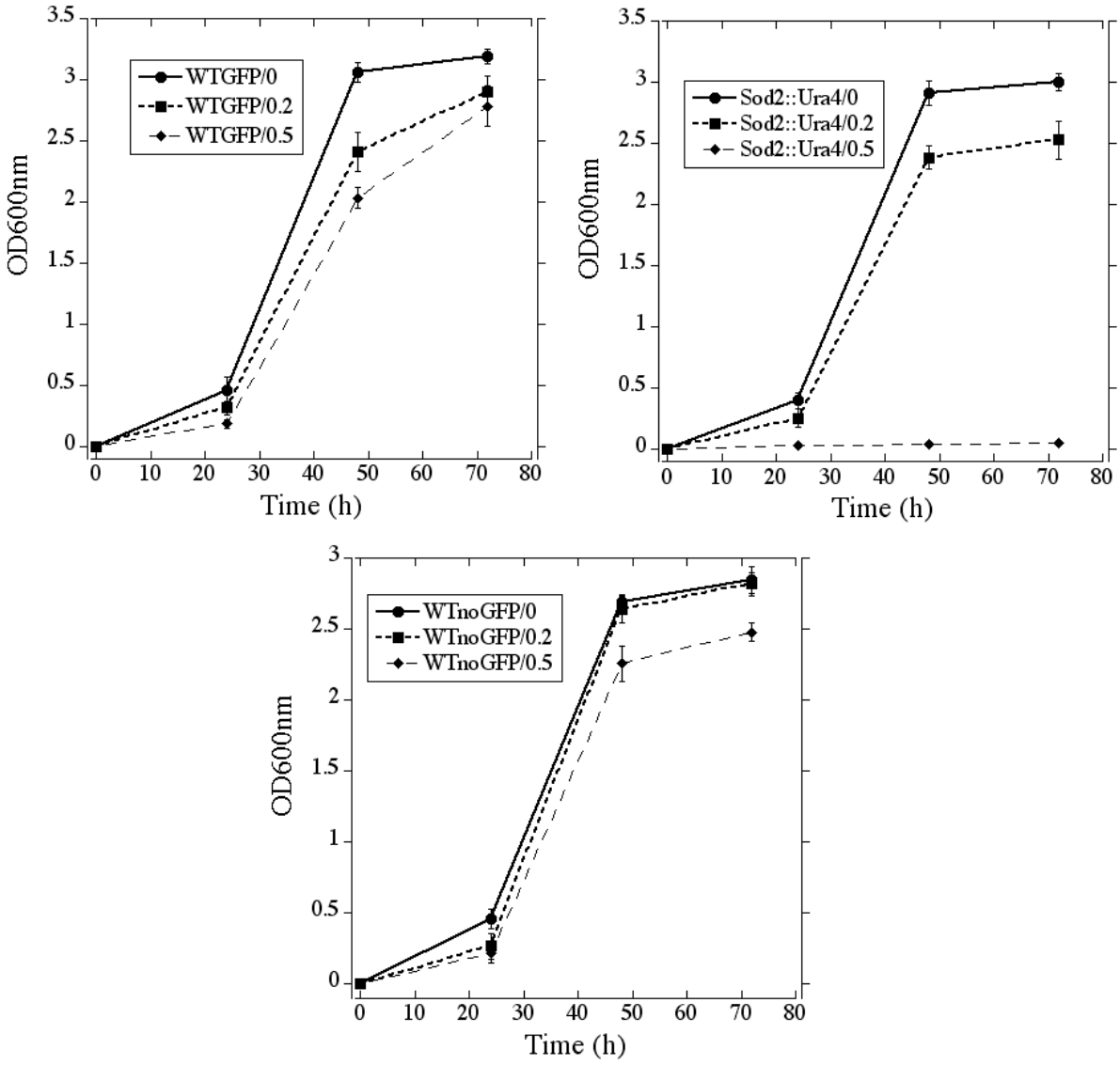
WTGFP/0
WTGFP/0.2
WTGFP/0.5
OD600nm
Time (h)
Sod2::Ura4/0
Sod2::Ura4/0.2
Sod2::Ura4/0.5
OD600nm
Time (h)
WTnoGFP/0
WTnoGFP/0.2
WTnoGFP/0.5
OD600nm
Time (h)

Fig. 4 Supplementary (A-D). Growth of *S. pombe* containing wild type and TM IV mutant sod2 on solid media containing various concentrations of LiCl. Samples of stationary phase cultures of the various yeast strains were taken and were serially diluted 10-fold. These were spotted onto minimal media plates supplemented with LiCl at the concentration indicated. Plates were then incubated for 4-5 days at 30^{o} C. Sod2(WT) refers to *S. pombe* transformed with pREP-41sod2GFP without any mutations. *sod2::ura4* is *S. pombe* with the sod2 knockout described earlier (3). Other designations are the *sod2::ura4* yeast strain transformed with pREP-41sod2GFP with the indicated point mutation in sod2 (panel **A-D**). Results are typical of at least 3 experiments

A

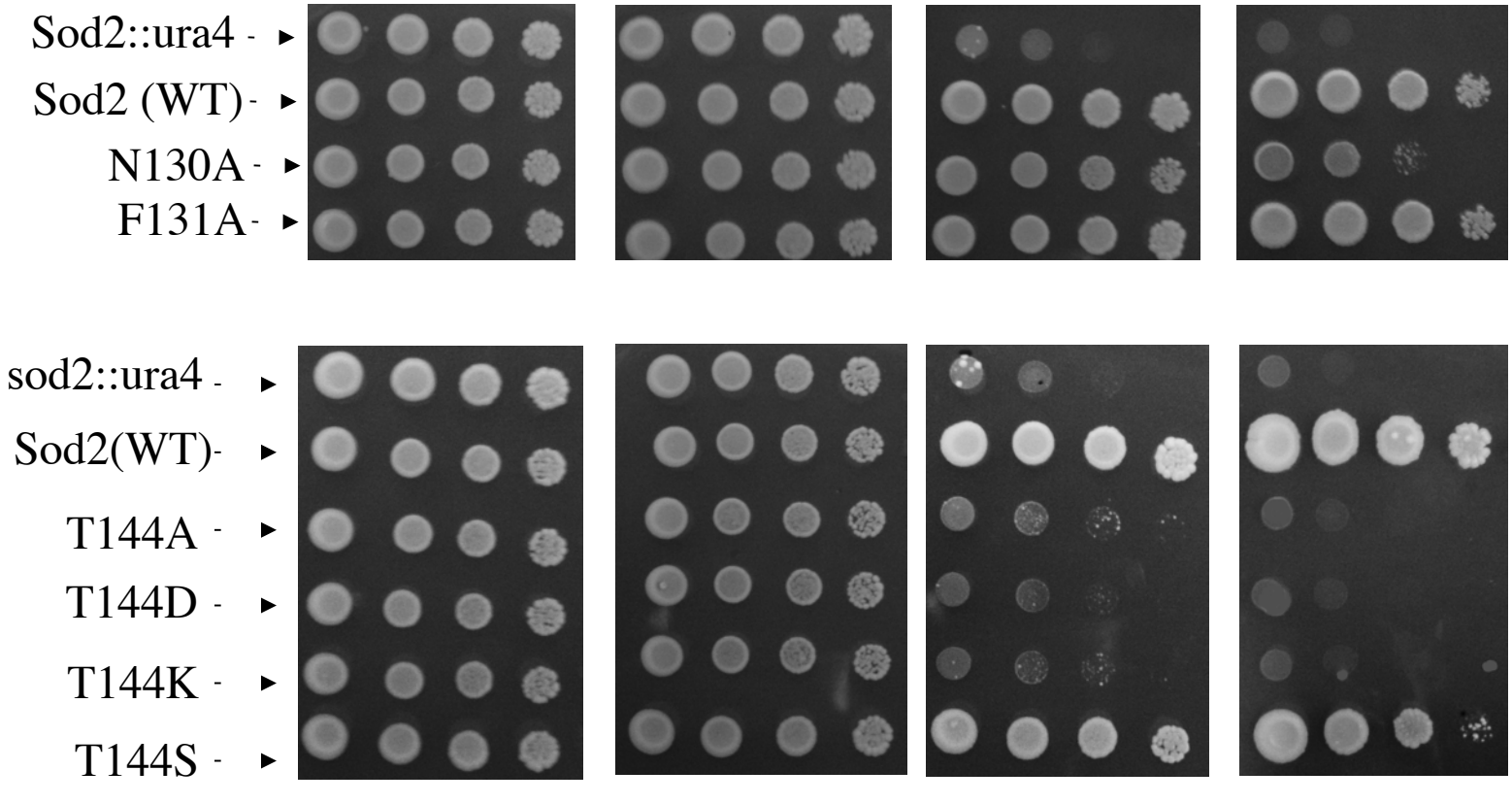
Sod2::ura4
Sod2 (WT)
N130A
F131A
sod2::ura4
Sod2(WT)
T144A
T144D
T144K
T144S
0
2
5
10
[LiCl] mM

B

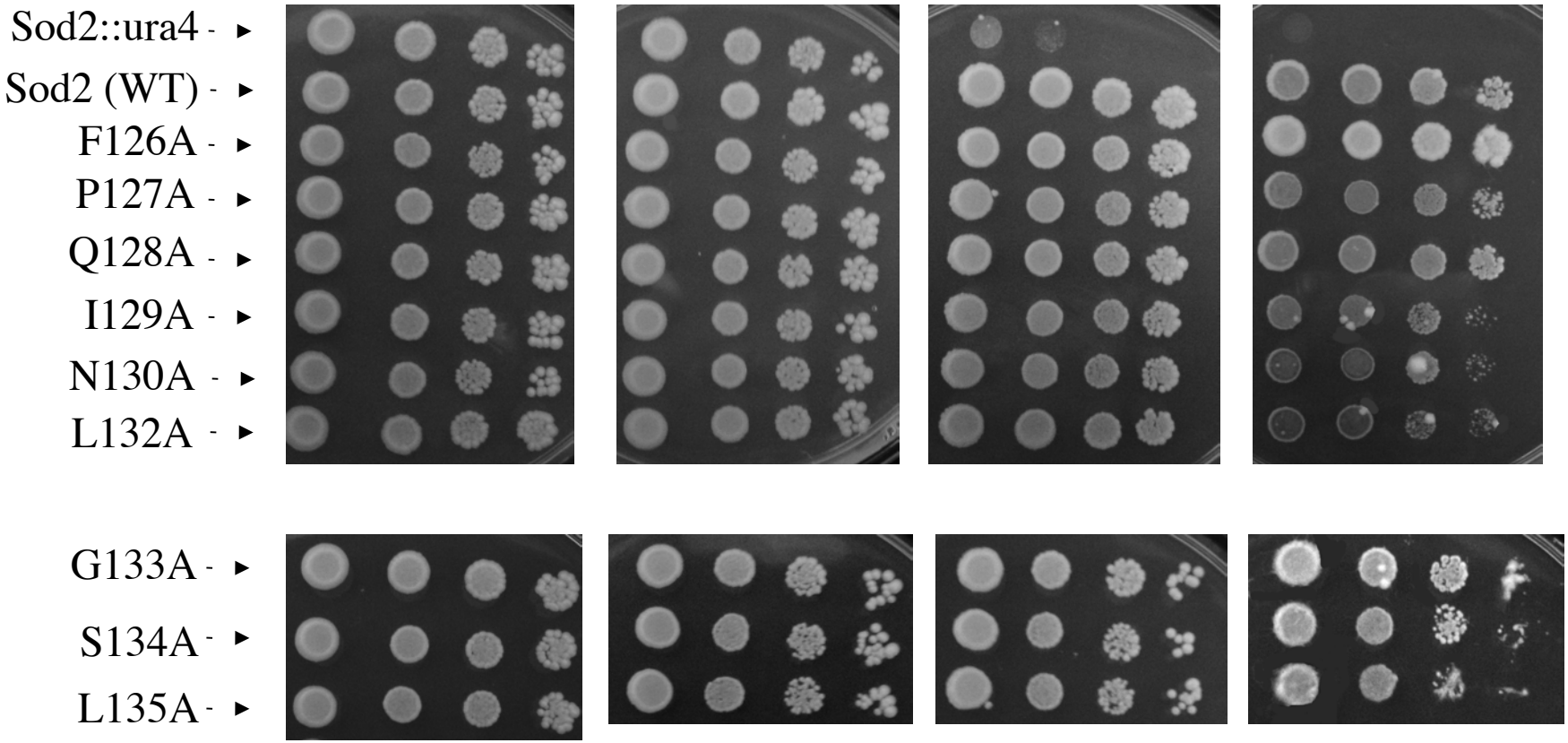
Sod2::ura4
Sod2 (WT)
F126A
P127A
Q128A
I129A
N130A
L132A
G133A
S134A
L135A
0
2
5
10
[LiCl] mM

C

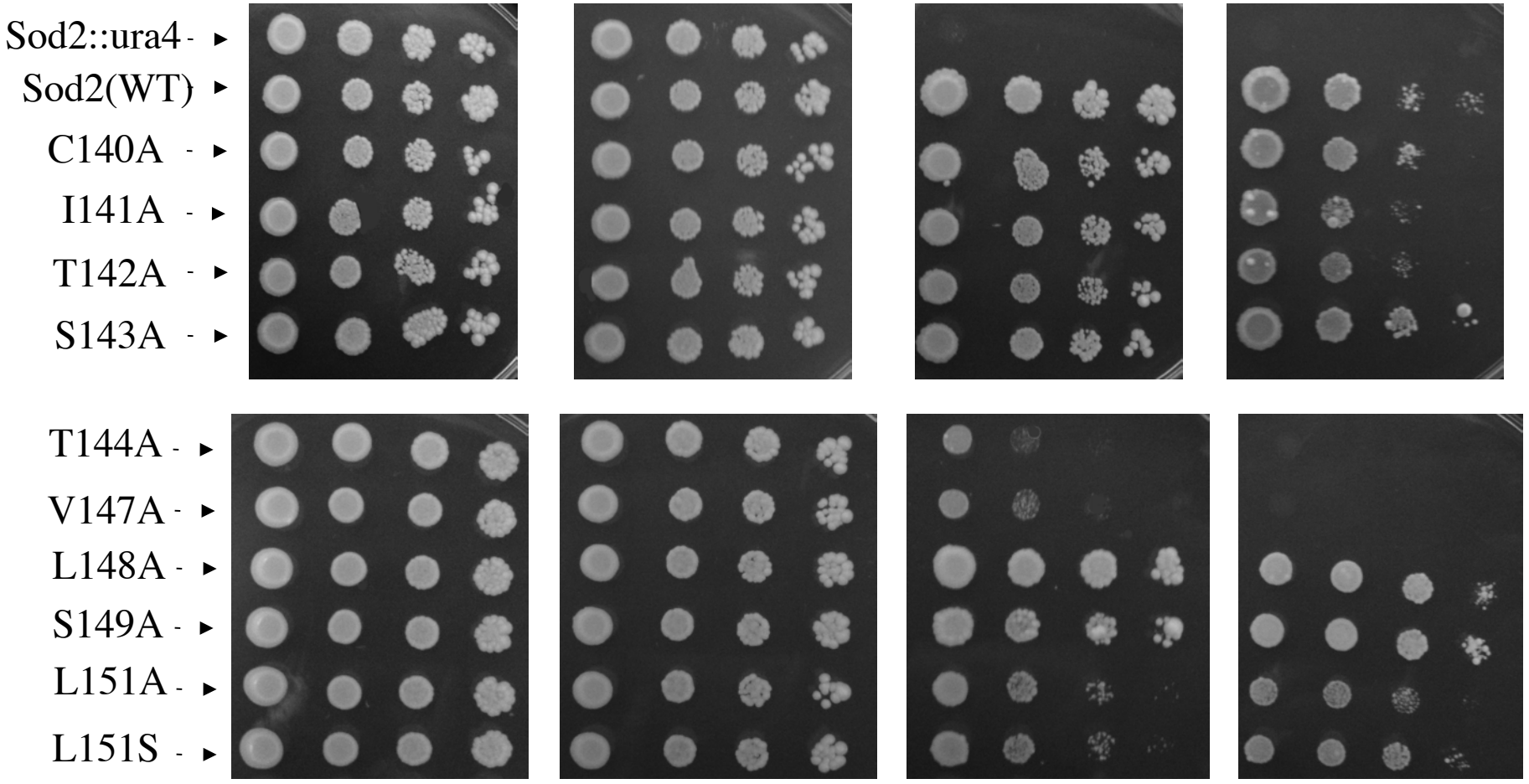
Sod2::ura4
Sod2(WT)
C140A
I141A
T142A
S143A
T144A
V147A
L148A
S149A
L151A
L151S
0
2
5
10
[LiCl] mM

D

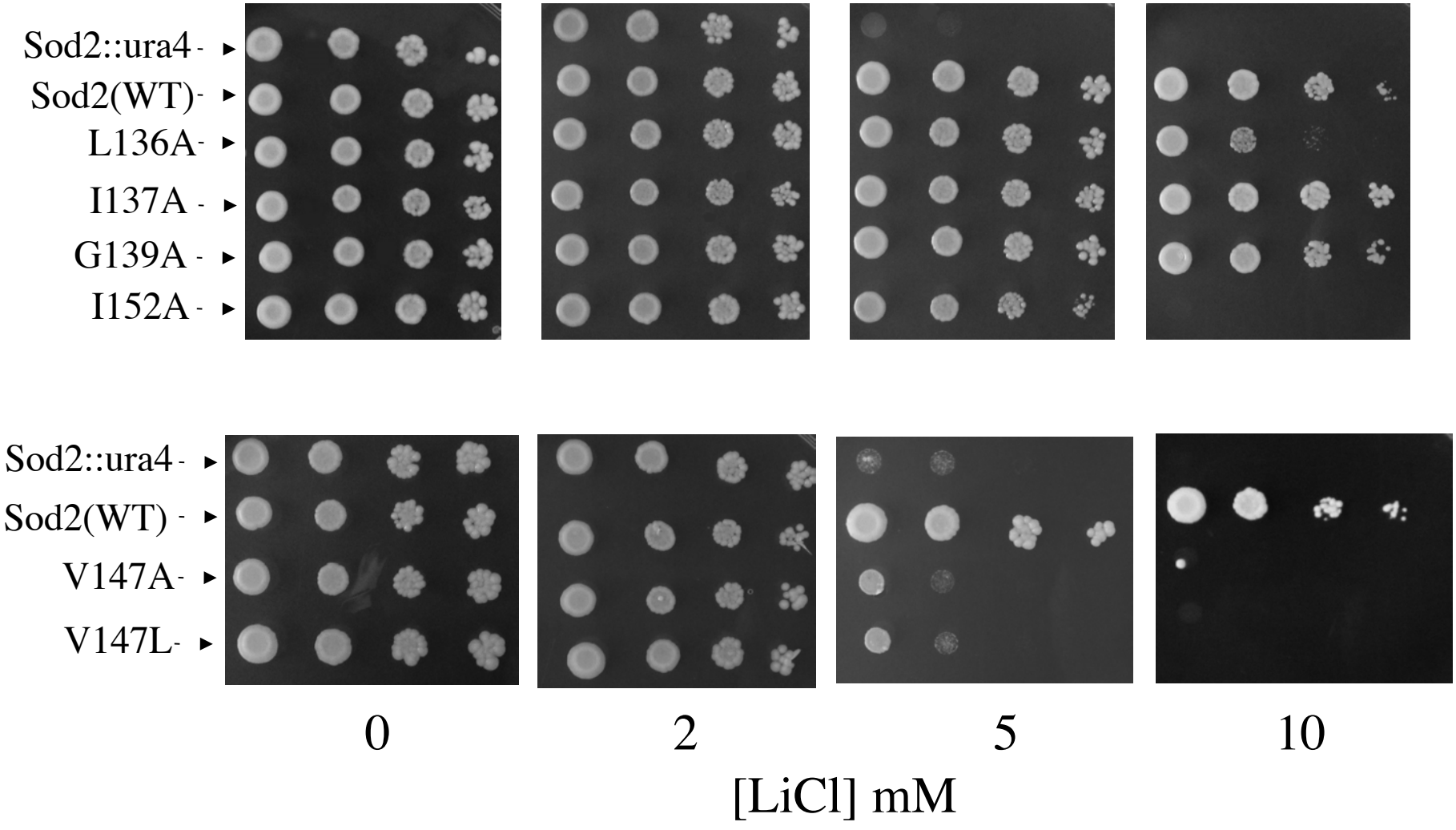
Sod2::ura4-
Sod2(WT)-
L136A-
I137A-
G139A-
I152A-
Sod2::ura4-
Sod2(WT)-
V147A-
V147L-
0
2
5
10
[LiCl] mM

A

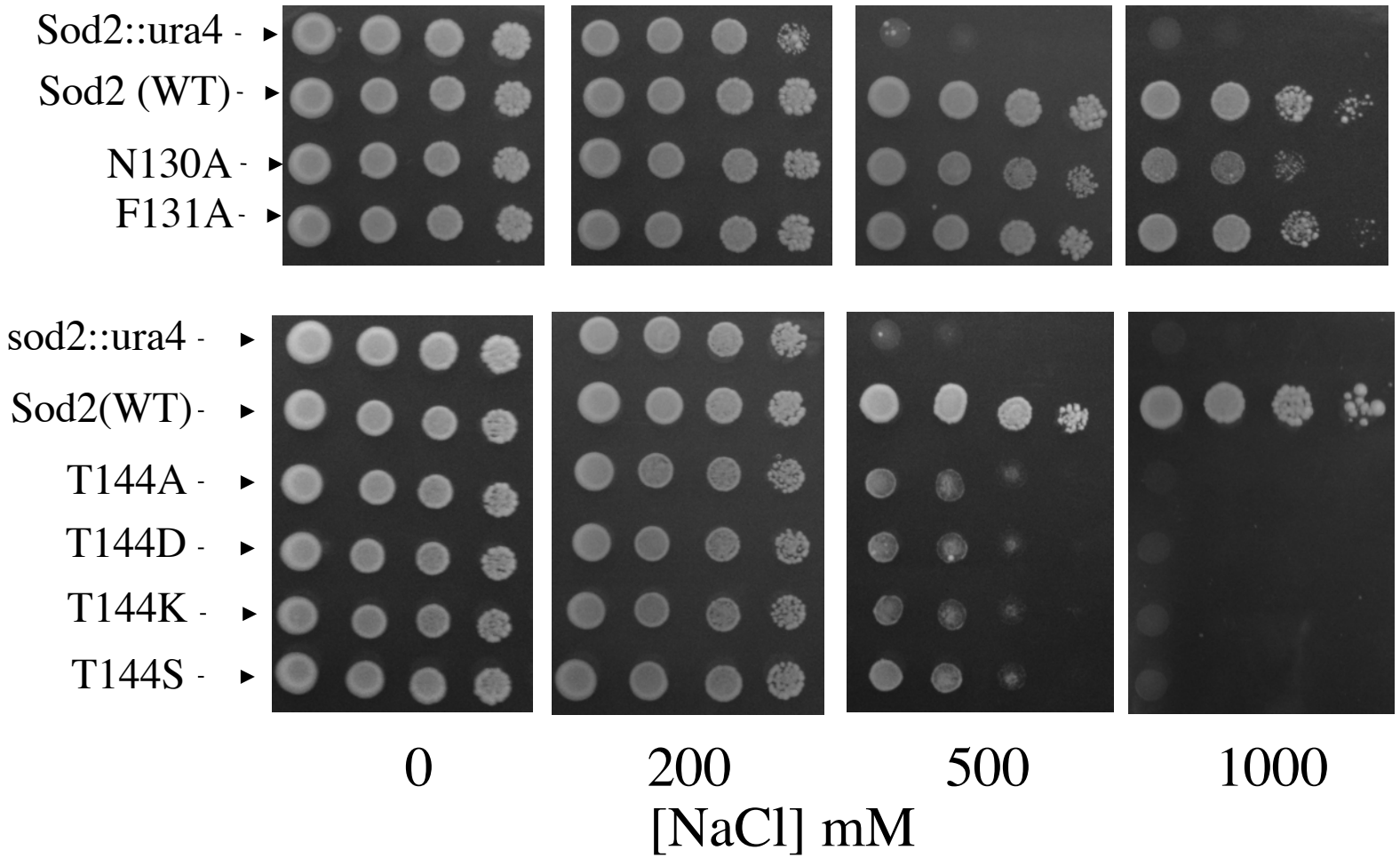

Fig. 5 Supplementary (A-D). Growth of *S. pombe* containing wild type and TM IV mutant sod2 on solid media as described in supplemental Fig. 4, except containing the indicated concentrations of NaCl. Results are typical of at least 3 experiments.

B

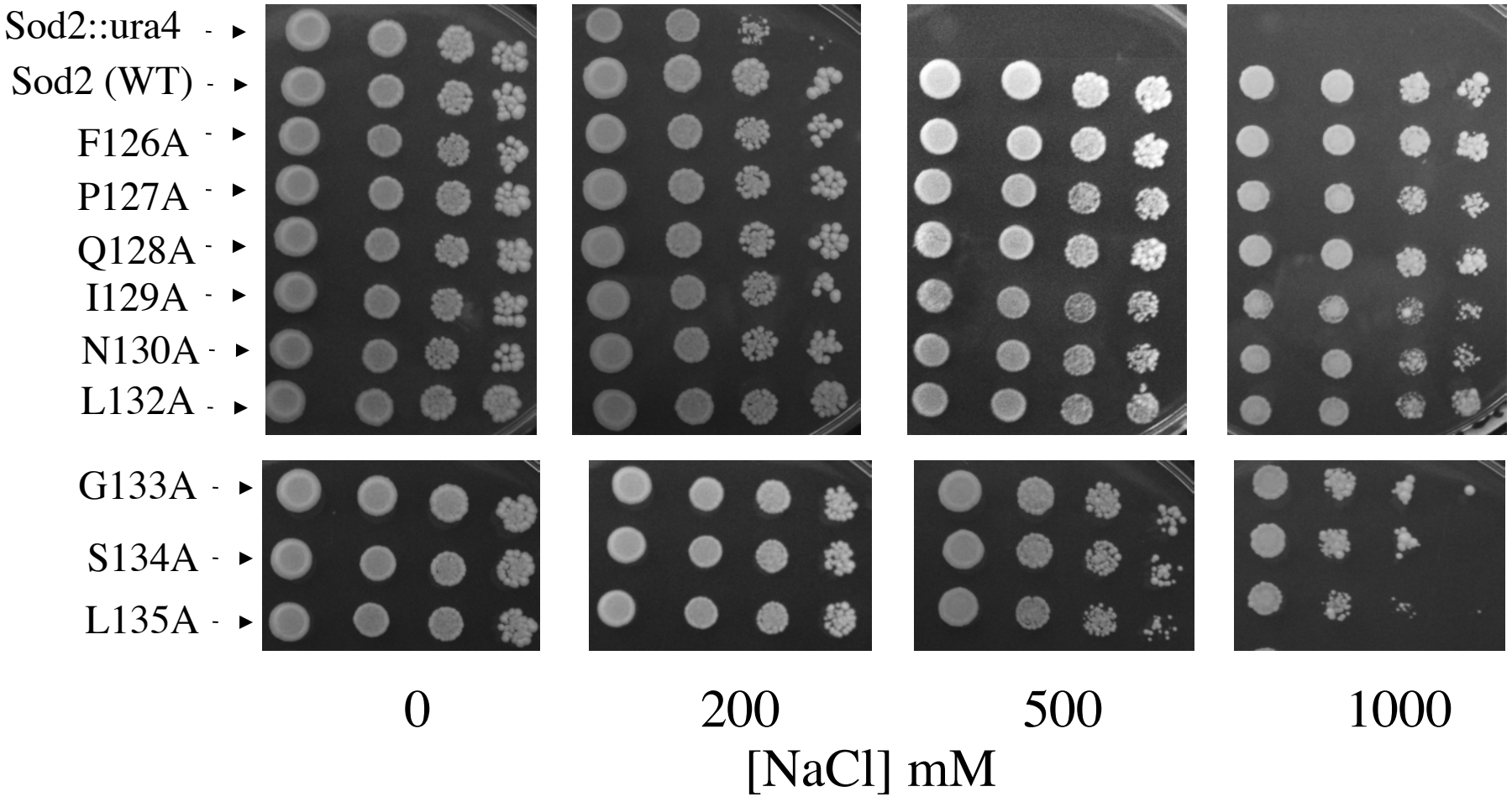
Sod2::ura4
Sod2 (WT)
F126A
P127A
Q128A
I129A
N130A
L132A
G133A
S134A
L135A
0
200
500
1000
[NaCl] mM

Fig. 5B.

C

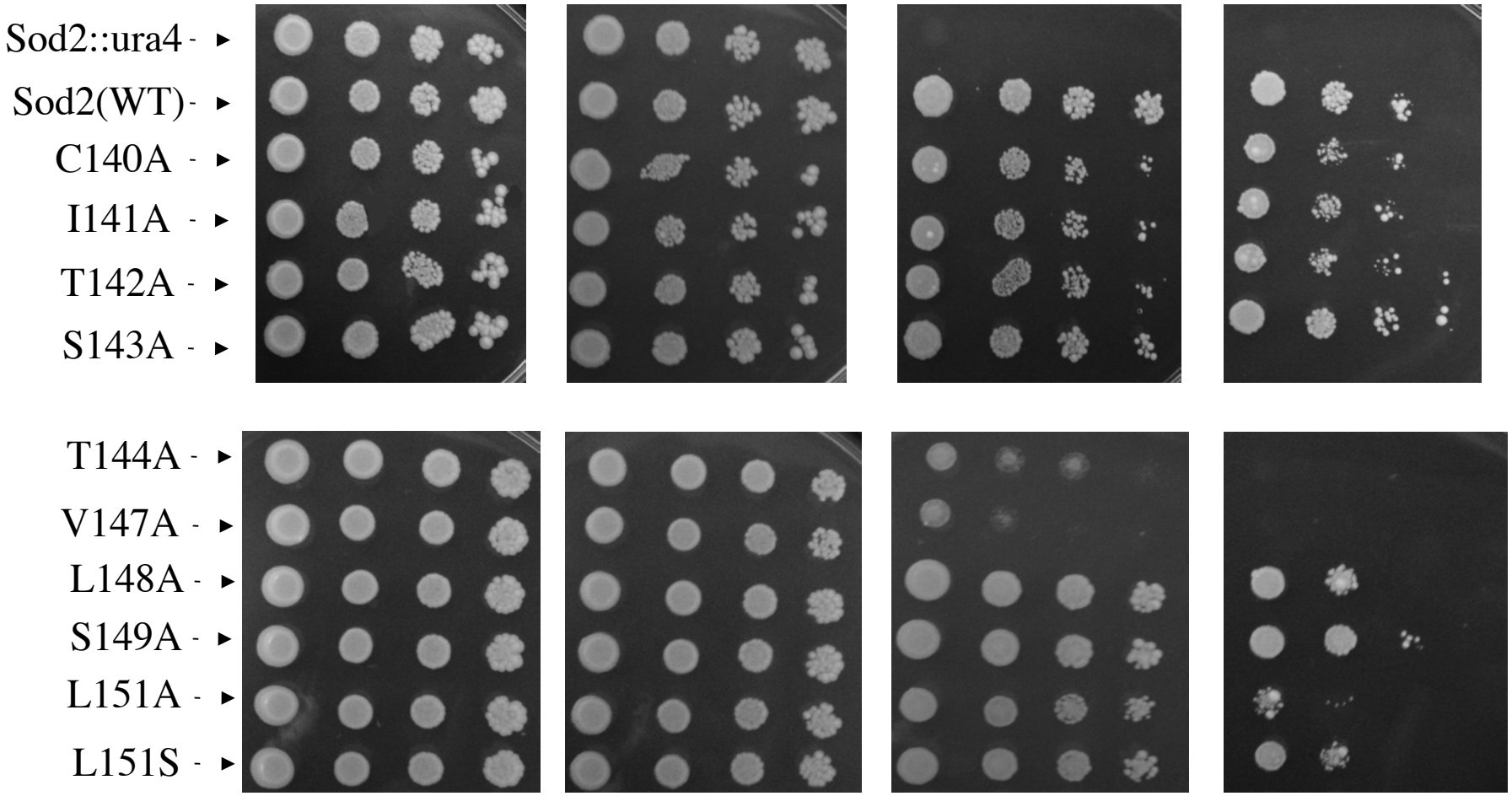
Sod2::ura4
Sod2(WT)
C140A
I141A
T142A
S143A
T144A
V147A
L148A
S149A
L151A
L151S
0
200
500
1000
[NaCl] mM

Fig. 5C.

D

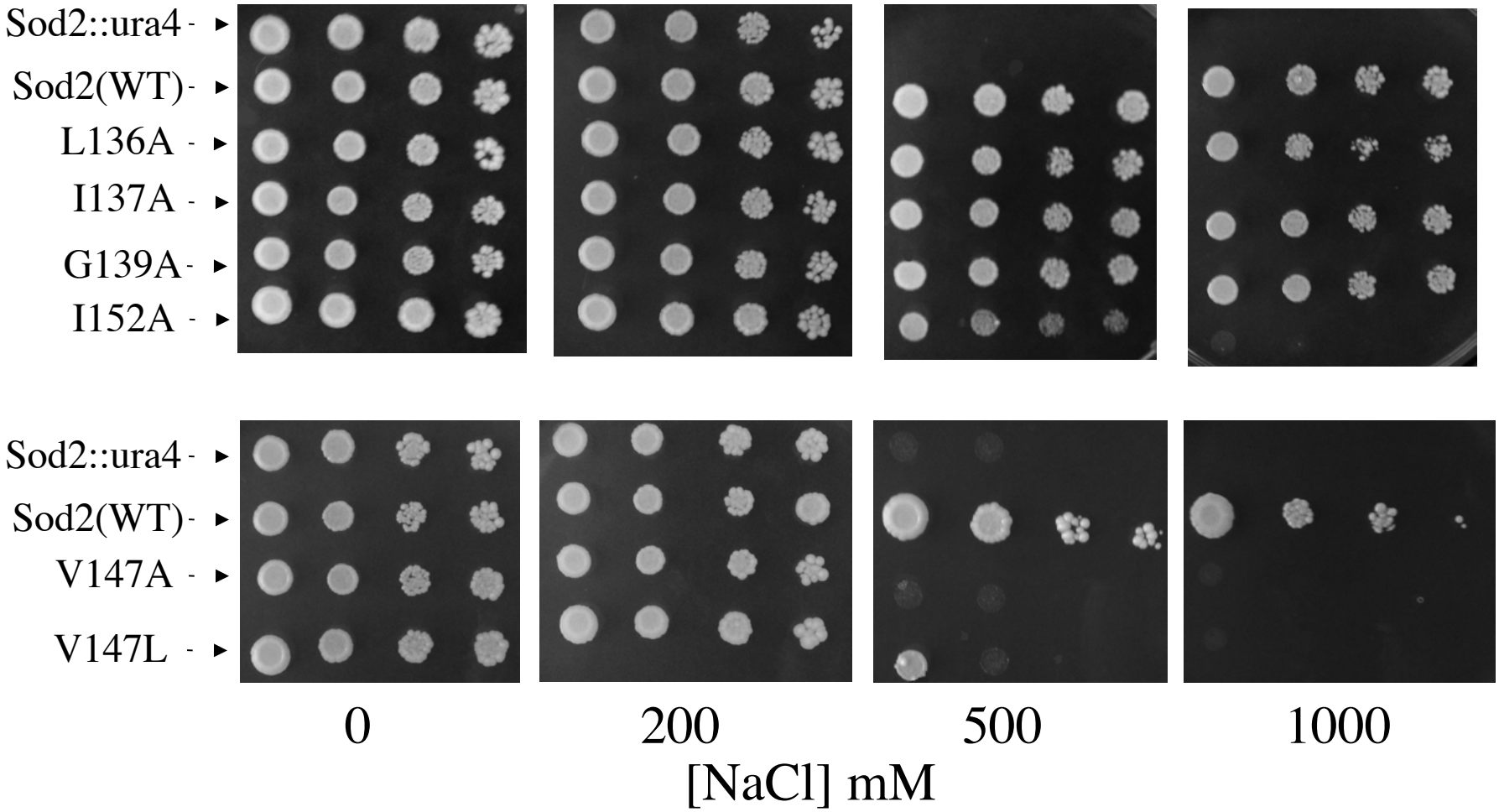
Sod2::ura4
Sod2(WT)
L136A
I137A
G139A
I152A
Sod2::ura4
Sod2(WT)
V147A
V147L
0
200
500
1000
[NaCl] mM

Fig. 5D.

Fig 6

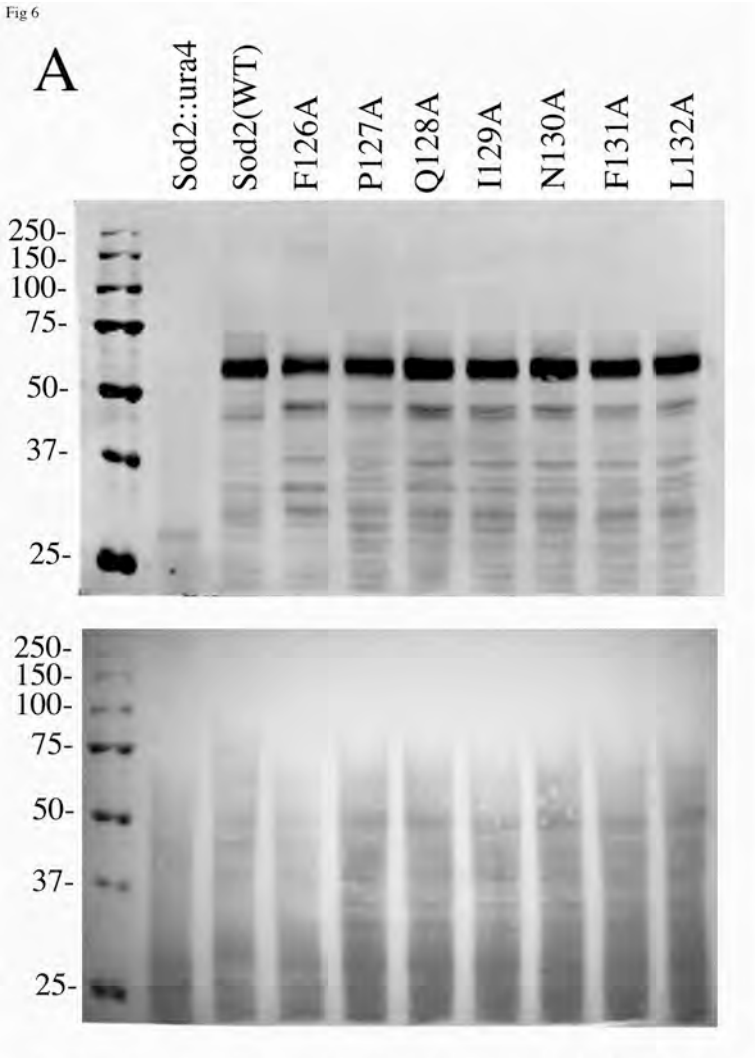

Fig. 6 Supplementary. Western blot analysis of expression levels of sod2 wild type and mutant containing S. pombe. Cell extracts from S. pombe strains separated by SDS-PAGE and were blotted with anti-GFP antibody. Molecular weight markers are indicated. A-D, cell extracts of sod2::ura4: untransformed (sod2::ura4); transformed with wild type (WT) sod2 protein; or transformed with sod2 proteins with the mutation indicated. Cell extracts were made as described in the "Materials and Methods". Upper panel, western blot; lower panel, Ponceau S staining of blot prior to immunoreaction.

Fig 6B

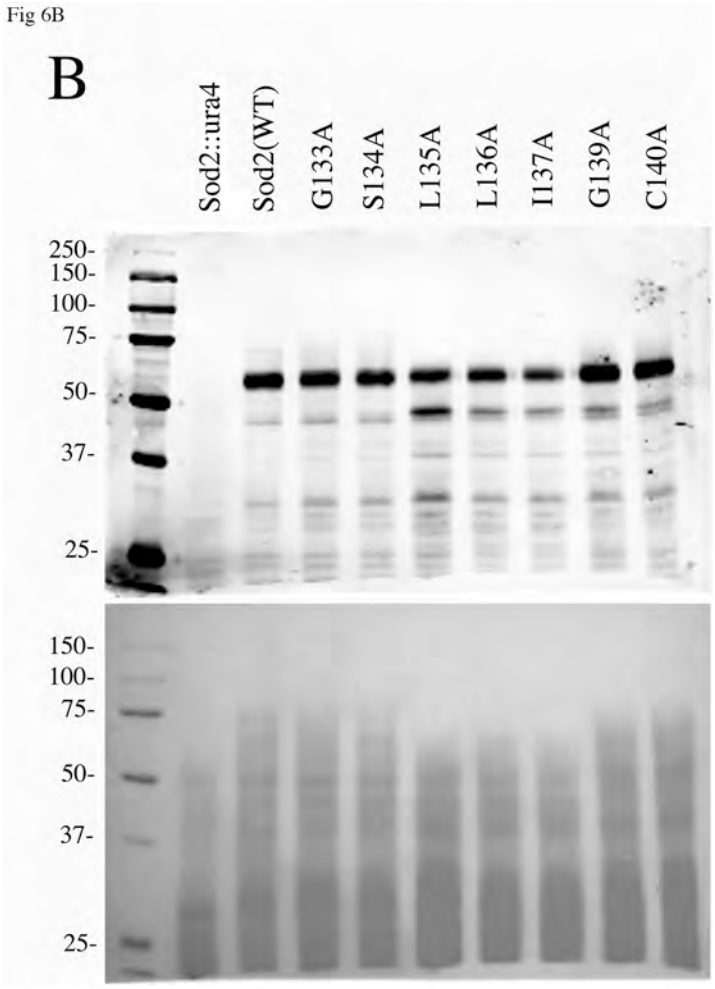

Fig. 6B Supplementary. Western blot analysis of expression levels of sod2 wild type and mutant containing S. pombe.

Fig 6C

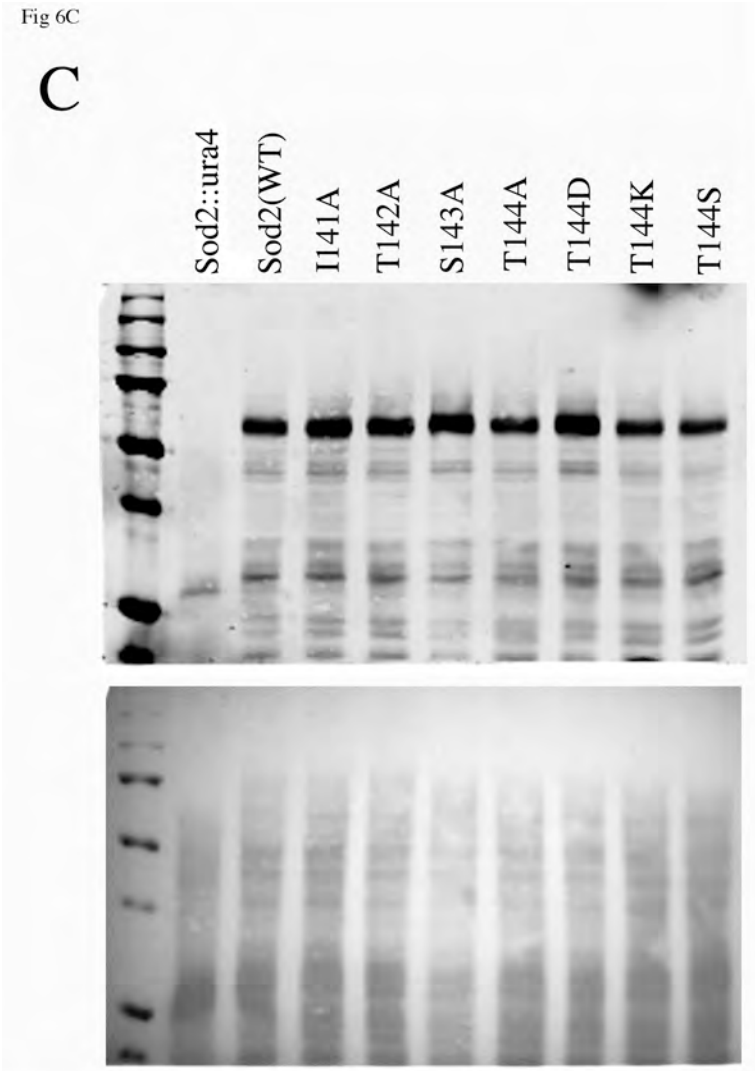

Fig. 6C Supplementary. Western blot analysis of expression levels of sod2 wild type and mutant containing S. pombe.

D

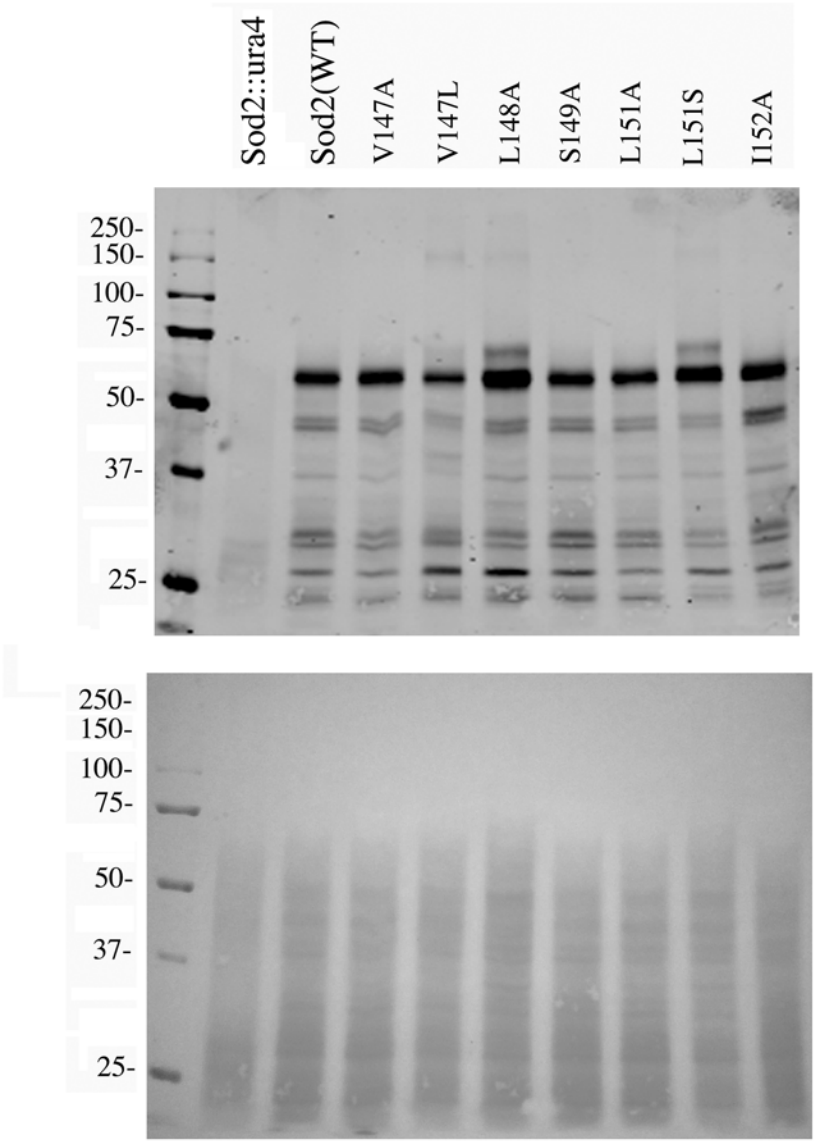

Fig. 6D Supplementary. Western blot analysis of expression levels of sod2 wild type and mutant containing S. pombe.

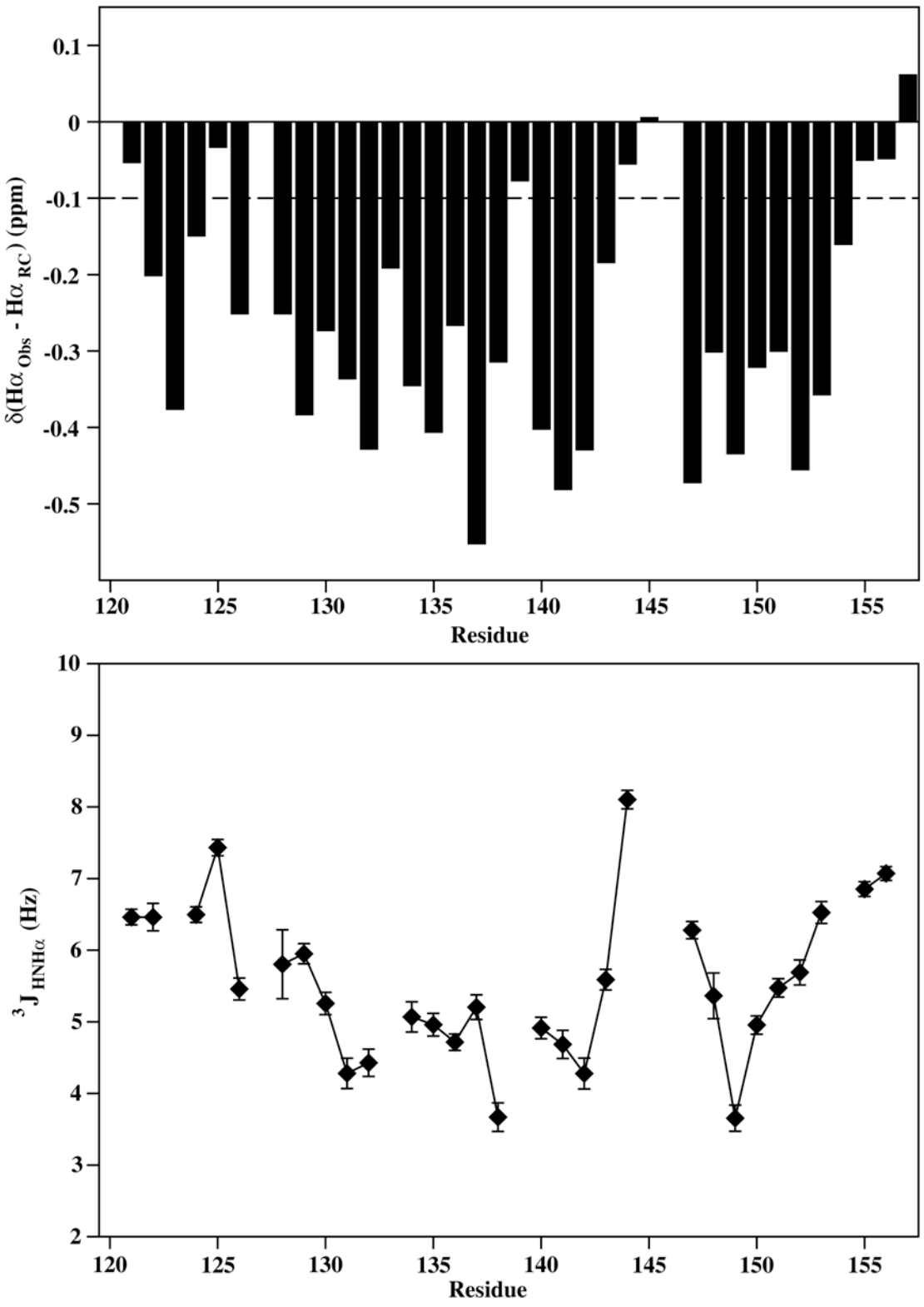

Fig. S7. (Top) Chemical shift index prediction of sod2 TMIV secondary structure. Contiguous regions with deviations lower than -0.1 ppm (dotted line) from random coil chemical shifts indicate alpha-helical structure. Glycine chemical shifts were averaged if two Hα peaks are resolved. (Bottom) $^{3}J_{HNH\alpha}$ coupling constants calculated for the peptide from a 3D HNHA NMR spectrum. Regions approximately < 5 Hz suggest alpha helical structure, and > 8 Hz extended structure. Missing values are glycines or were not calculated due to peak overlap.

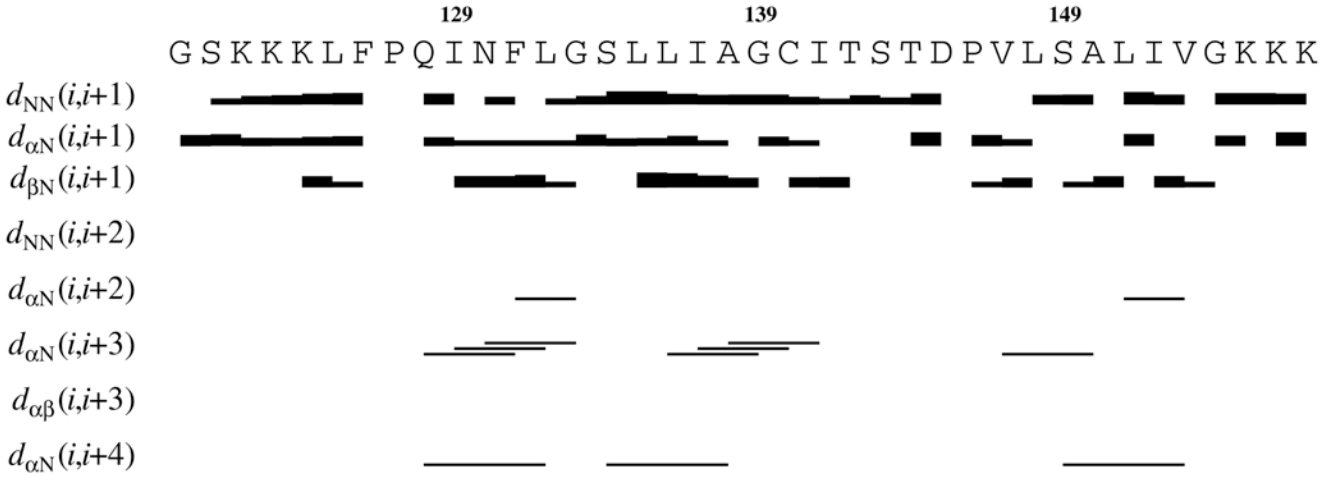

Fig. S8. Summary of NOE distances observed in a 3D ^{15}N NOESY-HSQC spectrum of sod2 TMIV. Regions containing (i,i+3) and (i,i+4) contacts suggest helical structure.

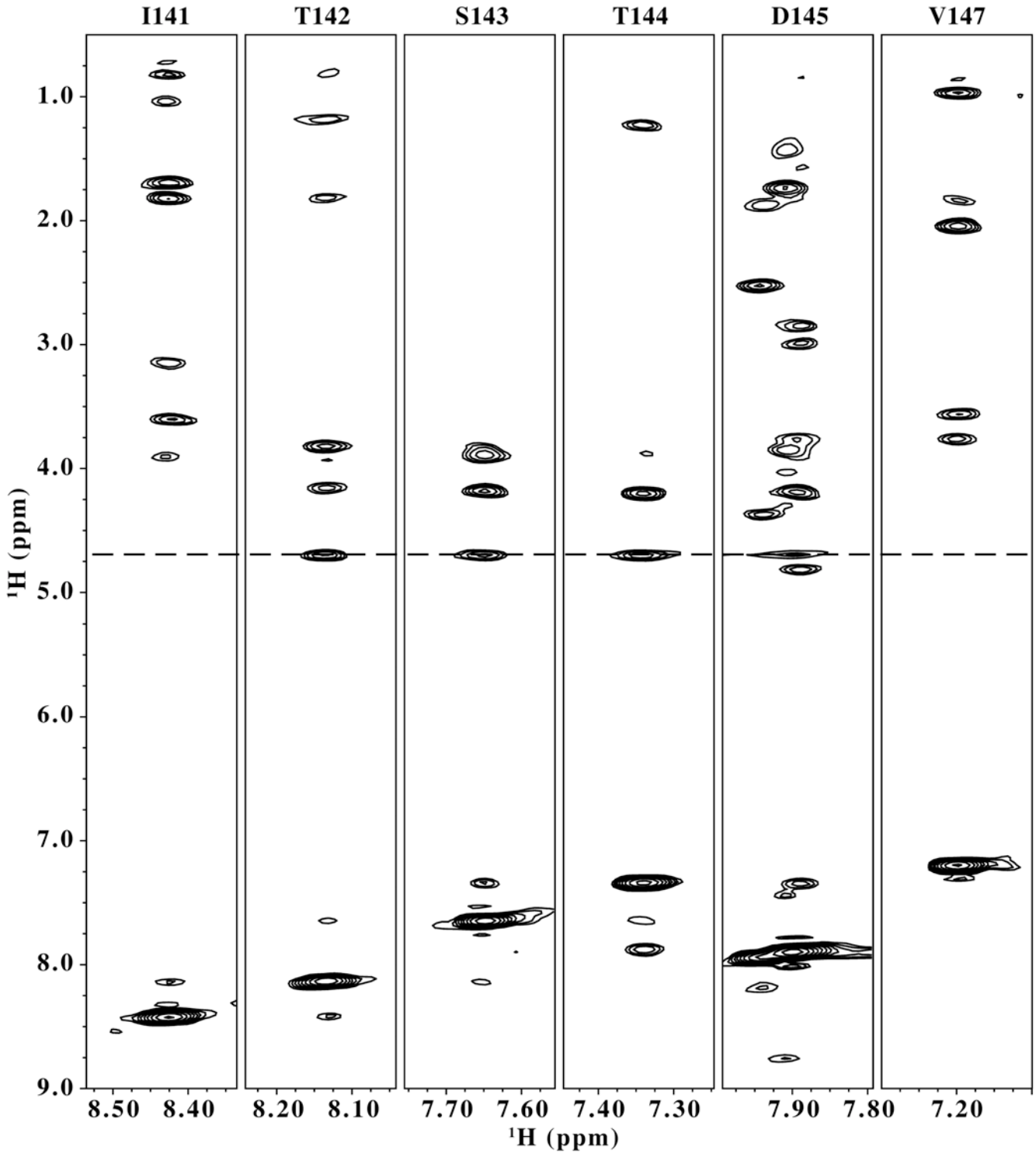

Fig. S9. 3D ^{15}N NOESY-HSQC strip plot of the residues in the central extended region of sod2 TMIV showing exchange peaks with water (dotted line).

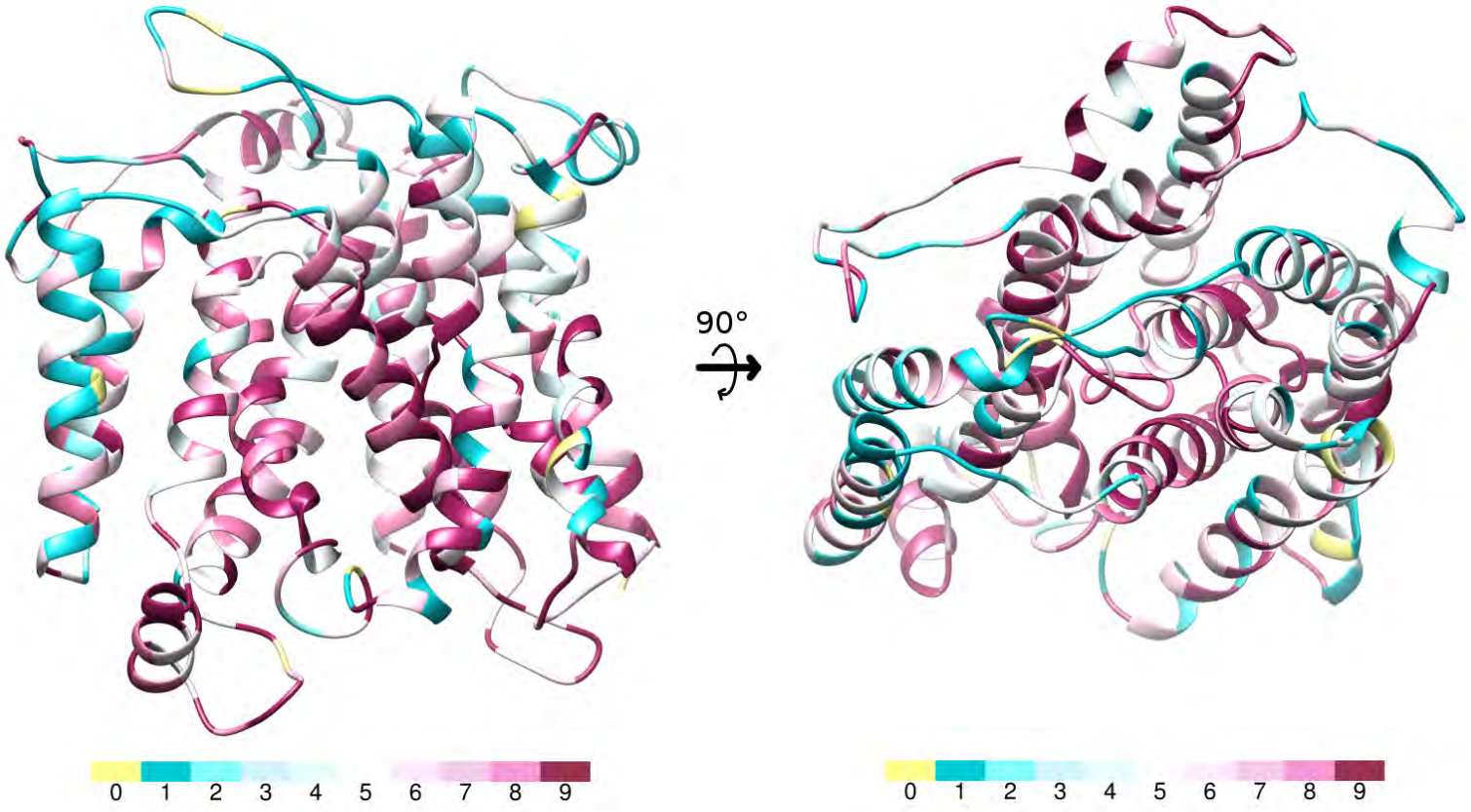

Fig 10 supplemental. ConSurf conservation mapping on sod2 homology model. The ConSurf server (40) was used to create a multiple sequence alignment and calculate the overall conservation score for each residue in sod2. This conservation score (0-9) was mapped onto the homology model of sod2 using a colour scale. Internal regions of the protein important for transport show generally higher levels of conservation and external region of the protein are less well conserved.
The key residues in TM IV have either the highest conservation score, 9 (T144, D145, P146) or the second highest, 8 (V147).